HHS Public Access

Author manuscript

Dev Cell. Author manuscript; available in PMC 2018 April 24.

Published in final edited form as:

Dev Cell. 2017 April 24; 41(2): 143–156.e6. doi:10.1016/j.devcel.2017.03.025.

Mps1 regulates kinetochore-microtubule attachment stability via the Ska complex to ensure error-free chromosome segregation

John Maciejowski[1,2], **Hauke Drechsler**[3], **Kathrin Grundner-Culemann**[4,5], **Edward R. Ballister**[6,7], **Jose-Antonio Rodriguez-Rodriguez**[1], **Veronica Rodriguez-Bravo**[1,8], **Mathew J.K. Jones**[1], **Emily Foley**[2,8], **Michael A. Lampson**[6,7], **Henrik Daub**[4,5], **Andrew D. McAinsh**[3], and **Prasad V. Jallepalli**[1,2,*]

[1]Molecular Biology Program, Sloan Kettering Institute, Memorial Sloan Kettering Cancer Center, New York, NY, 10065, USA

[2]Louis V. Gerstner, Jr. Graduate School of Biomedical Sciences, Memorial Sloan Kettering Cancer Center, New York, NY, 10065, USA

[3]Centre for Mechanochemical Cell Biology, Division of Biomedical Science, Warwick Medical School, University of Warwick, Coventry CV4 7AL, UK

[4]Cell Signaling Group, Department of Molecular Biology, Max Planck Institute of Biochemistry, Am Klopferspitz 18, 82152 Martinsried, Germany

[5]Evotec (München) GmbH, Am Klopferspitz 19a, 82152 Martinsried, Germany

[6]Department of Biology, University of Pennsylvania, Philadelphia, PA 19104, USA

[7]Graduate Group in Biochemistry and Molecular Biophysics, University of Pennsylvania, Philadelphia, PA 19104, USA

[8]Cell Biology Program, Sloan Kettering Institute, Memorial Sloan Kettering Cancer Center, New York, NY, 10065, USA

SUMMARY

The spindle assembly checkpoint (SAC) kinase Mps1 not only inhibits anaphase but also corrects erroneous attachments that could lead to missegregation and aneuploidy. However, Mps1's error correction-relevant substrates are unknown. Using a chemically tuned kinetochore-targeting assay, we show that Mps1 destabilizes microtubule attachments (K-fibers) epistatically to Aurora B, the other major error-correcting kinase. Through quantitative proteomics, we identify multiple sites of Mps1-regulated phosphorylation at the outer kinetochore. Substrate modification was microtubule-

*Corresponding author & lead contact: jallepap@mskcc.org.

AUTHOR CONTRIBUTIONS

J.M., E.R.B., J.-A.R.-R., V.R.-B., M.J.K.J., and E.F. performed molecular biology, cell imaging, and biochemical studies and analyzed data. K.G.-C. H. performed SILAC mass spectrometry experiments and analyzed data. H. Dreschler performed biochemical and TIRF imaging studies and analyzed data. P.V.J., A.D.M., H. Daub, and M.A.L. planned and supervised research, analyzed data, and secured funding. P.V.J., A.D.M., and H. Daub wrote the paper with input from all authors.

sensitive and opposed by PP2A-B56 phosphatases that stabilize chromosome-spindle attachment. Consistently, Mps1 inhibition rescued K-fiber stability after depleting PP2A-B56. We also identify the Ska complex as a key effector of Mps1 at the kinetochore-microtubule interface, as mutations that mimic constitutive phosphorylation destabilized K-fibers in vivo and reduced the efficiency of the Ska complex's conversion from lattice diffusion to end-coupled microtubule binding in vitro. Our results reveal how Mps1 dynamically modifies kinetochores to correct improper attachments and ensure faithful chromosome segregation.

Graphical abstract

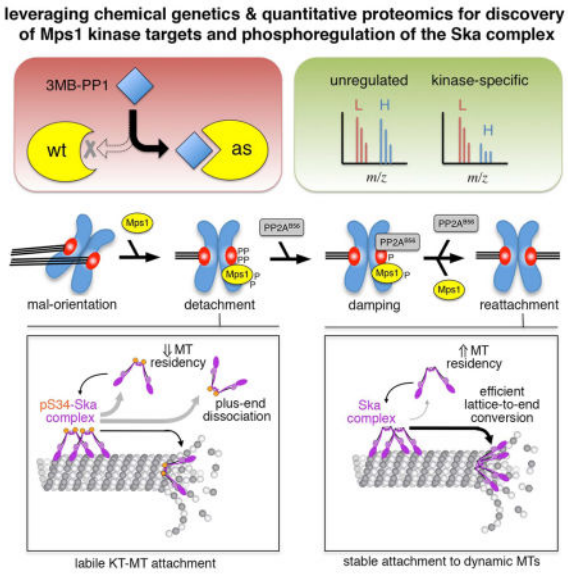

INTRODUCTION

Accurate chromosome segregation requires that all sister kinetochores are attached to stabilized microtubule bundles (also called K-fibers) from opposite spindle poles before anaphase onset (Tanaka, 2010). To enforce this requirement, the ubiquitin ligase activity of the anaphase-promoting complex/cyclosome (APC/C) is restrained by the spindle assembly checkpoint (SAC), a surveillance system that monitors the integrity of chromosome-spindle linkages (Foley and Kapoor, 2013; London and Biggins, 2014). In brief, unattached or mal-oriented kinetochores recruit SAC mediators and elaborate a multi-subunit anaphase inhibitor known as the mitotic checkpoint complex (MCC), which binds and inhibits the APC/C coactivator Cdc20 (Foley and Kapoor, 2013; London and Biggins, 2014). As a result securin, cyclin B, and other APC/C-Cdc20 substrates are protected from ubiquitin-mediated proteolysis, preventing sister chromatid separation and mitotic exit.

In addition to delaying anaphase, a number of SAC mediators promote chromosome bi-orientation through direct regulation of kinetochore-microtubule attachments. For instance, the pseudokinase BubR1 stabilizes K-fibers by recruiting B56-associated isoforms of protein phosphatase 2A (PP2A-B56) to kinetochores (Foley et al., 2011; Kruse et al., 2013; Suijkerbuijk et al., 2012; Xu et al., 2013). Conversely, the Aurora B kinase (a key

component of the inner centromere-localized chromosome passenger complex (CPC)) destabilizes improper attachments via phosphorylation of the Ndc80 complex, the microtubule depolymerase MCAK, and other substrates (Kelly and Funabiki, 2009; Lampson and Cheeseman, 2011; Tanaka, 2010). A third example involves the SAC kinase Mps1, whose depletion or inhibition by small molecules strongly impedes the correction of mal-oriented chromosomes (Hewitt et al., 2010; Maciejowski et al., 2010; Santaguida et al., 2010). However, the underlying substrates and molecular mechanisms that explain this function of Mps1 are unclear. One prominent proposal is that Mps1 directly phosphorylates the CPC subunit Borealin, thereby stimulating Aurora B's intrinsic kinase activity (Jelluma et al., 2008b). However, neither *MPS1*-null cells nor mitotic cells treated with Mps1 inhibitors exhibit decreased phosphorylation of canonical Aurora B substrates such as histone H3 or CENP-A (Hewitt et al., 2010; Maciejowski et al., 2010; Santaguida et al., 2010), nor is there evidence that the putative phosphoacceptor sites in Borealin are modified *in vivo* (Jelluma et al., 2008b). Collectively these and related data in yeast (Maure et al., 2007) raise important questions about how Mps1 promotes chromosome bi-orientation relative to the CPC, as well as the identity of Mps1's relevant substrates and their mechanisms of phosphoregulation.

We have used chemical biology, quantitative mass spectrometry, cell-based functional assays, and single-molecule biophysics to investigate Mps1's role in chromosome bi-orientation and error correction. Epistasis experiments reveal that kinetochore-localized Mps1 can destabilize microtubule attachments directly, even if Aurora B is inhibited. As a result, the formation of stable bipolar attachments requires reversal of Mps1-catalyzed phosphorylation by PP2A-B56 phosphatases (Foley et al., 2011) and exclusion of Mps1 from metaphase kinetochores (Hiruma et al., 2015; Jelluma et al., 2010; Ji et al., 2015). Through global phosphoproteomics, we discovered that Mps1 directly modifies the hinge region of the Ska complex, which tethers kinetochores to dynamic plus ends of microtubules and enables chromosome movement to be powered by conformational energy stored in microtubule polymers (Schmidt et al., 2012; Welburn et al., 2009). Phosphomimetic hinge mutation reduced the efficiency of the Ska complex's conversion from lattice diffusion to end-coupled microtubule binding *in vitro* and destabilized K-fibers *in vivo*, resulting in delayed anaphase onset, chromosome missegregation, and cell death. Together these results illuminate how Mps1 regulates the mechanical properties of the kinetochore, so that bi-orientation not only switches off the SAC, but also stabilizes the kinetochore's grip on dynamic microtubule ends.

RESULTS

Targeting Mps1 to metaphase kinetochores destabilizes microtubule attachment and disrupts chromosome alignment epistatically to Aurora B

Substantial evidence suggests that bipolar attachment (also termed bi-orientation) prevents error-correcting kinases from destabilizing the kinetochore-microtubule interface, thus ensuring that only improper attachments are targeted for ablation (Lampson and Cheeseman, 2011; Tanaka, 2010). For example, tension across metaphase kinetochores increases their distance from the inner centromere, which decreases CPC-dependent phosphorylation and

promotes stable binding to microtubules, unless Aurora B itself is repositioned closer to the kinetochore (Liu et al., 2009; Welburn et al., 2010). Similarly, Mps1 cycles between the cytoplasm and unattached or mal-oriented kinetochores, but is largely excluded from bi-oriented kinetochores (Howell et al., 2004; Jelluma et al., 2010), in part due to Mps1's microtubule-competitive binding to the Ndc80 complex (Hiruma et al., 2015; Ji et al., 2015). While important for checkpoint signaling, this spatial regulation has not been linked to Mps1's emerging role in selective error correction (Hewitt et al., 2010; Maciejowski et al., 2010; Santaguida et al., 2010). To probe this issue, we took advantage of the temporal control afforded by rapamycin-induced dimerization (Ballister et al., 2014; Kuijt et al., 2014) to examine the effect of targeting Mps1 to metaphase kinetochores. This experimental design allowed us to separate Aurora B's upstream role in promoting Mps1's localization and activation at kinetochores (Nijenhuis et al., 2013; Santaguida et al., 2011; Saurin et al., 2011) from any downstream role as an Mps1 effector (Jelluma et al., 2008b). HeLa cell lines were engineered to express Mis12-GFP fused to three copies of FKBP (Ballister et al., 2014) and mCherry-Mps1 fused to the FKBP- and rapamycin-binding domain (FRB) of mTOR (Fig. 1A), thereby enabling ligand-dependent relocalization (Fig. S1) and activation of Mps1 via *trans* autophosphorylation (Kang et al., 2007). Within minutes of rapamycin addition, FRB-mCherry-Mps1 was targeted to kinetochores and triggered the misalignment of chromosomes that had previously congressed at the metaphase plate, blocking anaphase entry (Fig. S1A–B). This defect was accompanied by a sharp decrease in K-fiber integrity, as shown by brief cold treatment to depolymerize unstable microtubules before fixation (Rieder, 1981) and immunofluorescence microscopy (IFM) (Fig. 1B–C and Fig. S1C). We then performed chemical epistasis experiments in which cells were treated with reversine (an Mps1-selective inhibitor) (Santaguida et al., 2010) or ZM447439 (an Aurora B-selective inhibitor) (Ditchfield et al., 2003) before targeting Mps1 to metaphase kinetochores with rapamycin. Only reversine protected chromosomes from misalignment (Fig. 1D–E), demonstrating that Mps1 can destabilize attachments even when Aurora B is inhibited. Using phosphospecific antibodies to Dsn1 (Welburn et al., 2010), we confirmed that kinetochore-targeted Mps1 did not modify Aurora B target sites directly (Fig. 1F–G), in line with Mps1's and Aurora B's contrasting selectivity for acidic and basic residues on peptide substrates (Alexander et al., 2011; Dou et al., 2011; Hennrich et al., 2013).

Global quantitative proteomics reveals sites of Mps1-regulated phosphorylation at the outer kinetochore

Next we used chemical genetics (Maciejowski et al., 2010) and global phosphoproteomics (Oppermann et al., 2012) to identify Mps1's downstream targets with high confidence. This approach takes advantage of *MPS1*-null retinal pigment epithelial (RPE) cells reconstituted with the wildtype kinase ($Mps1^{wt}$) or an analog-sensitive allele ($Mps1^{as}$) (Maciejowski et al., 2010). Both cell lines were subjected to SILAC (stable isotope labeling by amino acids in culture), arrested in mitosis with spindle poisons, and treated with or without the bulky purine analog 3MB-PP1 (to inhibit $Mps1^{as}$) plus the proteasome inhibitor MG132 (to block anaphase and mitotic exit independently of the SAC; Fig. 2A). After pooling the SILAC-encoded cell lysates, chromatographically separated and enriched phosphopeptide fractions were prepared and analyzed by mass spectrometry (Oppermann et al., 2012). Over 27,000 phosphopeptides and 23,000 phosphosites were detected in four biological replicates of each

cell line (Fig. 2B). We leveraged the high level of phosphoproteome coverage to distinguish on-target (i.e., $Mps1^{as}$-specific) effects of 3MB-PP1 from potential off-target effects of the compound, which should manifest in both cell lines. For this purpose phosphorylation events quantified in at least two replicates of each cell line were statistically evaluated using SAM (Oppermann et al., 2012), revealing 19 phosphosites and 24 phosphopeptides that were significantly and greater than two-fold regulated in $Mps1^{as}$ cells but not in $Mps1^{wt}$ cells (estimated false-discovery rate (FDR) = 0%; Fig. S2A–B and Tables S1–S3). Gene ontology and STRING network analyses were used to contextualize these high-confidence Mps1 targets and mine our dataset for provisionally regulated phosphosites and phosphopeptides, that had been measured in fewer replicates, either on the same proteins or adjacent nodes in the network (Fig. 2C–D and Tables S1 and S2).

Overall Mps1-regulated phosphorylation was strongly biased towards outer kinetochore proteins involved in microtubule attachment, chromosome congression, and SAC signaling. As this group comprised both known and previously unidentified targets of Mps1, these findings not only validated our approach, but also provided a valuable resource for further mechanistic studies. For instance, we saw strong inhibition of Mps1 (TTK) autophosphorylation at multiple sites (Daub et al., 2008; Dou et al., 2011; Jelluma et al., 2008a; Kang et al., 2007; Mattison et al., 2007), as well as reduced phosphorylation of Bub1, BubR1 (BUB1B), and the Bub1 substrate histone H2A, which when modified on T121 recruits the cohesin protector Sgo1 to sister centromeres (Kawashima et al., 2010). These findings comport with our earlier observation that Mps1 recruits and maintains Bub1, BubR1, and more distal SAC transducers at kinetochores, and thus is required for centromeric H2A phosphorylation and Sgo1 localization (Hewitt et al., 2010; Maciejowski et al., 2010; Santaguida et al., 2010; Sliedrecht et al., 2010), as well as more recent evidence that Bub1 and BubR1 interact with Mps1-phosphorylated MELT motifs in KNL1 (CASC5), a large scaffold protein at the kinetochore (London et al., 2012; Shepperd et al., 2012; Yamagishi et al., 2012), and that Mps1 phosphorylates the yeast BubR1 ortholog Mad3 (Zich et al., 2016). While MELT motif phosphorylation was not detected without enriching KNL1, suggestive of low stoichiometry, we identified new Mps1-regulated phosphosites at the C-terminus of KNL1, which binds the Mis12 complex and targets KNL1 to kinetochores (Kiyomitsu et al., 2007). In metazoans this domain also recruits the RZZ complex, which leverages dynein-mediated transport to regulate SAC signaling and maturation of kinetochore-microtubule attachments (Barisic et al., 2010; Buffin et al., 2005; Gassmann et al., 2008; Kops et al., 2005). Consistently, our survey revealed Mps1-dependent modifications on the Rod (KNTC1) subunit of the RZZ complex, the dynein adapters Spindly (CCDC99) (Chan et al., 2009; Griffis et al., 2007) and CENP-F (Vergnolle and Taylor, 2007; Yang et al., 2005), and the light intermediate chain of cytoplasmic dynein (DYNC1LI1). Similar phosphoregulation was also seen for CENP-E, a plus end-directed motor essential for chromosome congression (Gudimchuk et al., 2013; Kim et al., 2008), and may explain the previous observation that Mps1 can stimulate CENP-E motility *in vitro* (Espeut et al., 2008). We also identified a novel Mps1-dependent site on Ska3 (also called C13orf3 or RAMA1), a subunit of the metazoan-specific Ska complex (Gaitanos et al., 2009; Raaijmakers et al., 2009; Welburn et al., 2009). Like the unrelated Dam1 complex in fungi, the Ska complex has been proposed to allow kinetochores to remain attached to

microtubule ends during depolymerization, a major driving force in mitotic chromosome movement (Gaitanos et al., 2009; Schmidt et al., 2012; Welburn et al., 2009). In contrast to the aforementioned proteins, phosphorylation of the HECT ubiquitin ligase HUWE1 (also called MULE) (Zhong et al., 2005) increased after Mps1 inhibition, implying indirect regulation through an Mps1-sensitive kinase or an Mps1-dependent phosphatase. As HUWE1-mediated degradation of Mcl1 is rate-limiting for apoptosis in mitotically arrested cells (Shi et al., 2011), our findings reveal molecular crosstalk between the SAC and cell death pathways that may influence the outcome of antimitotic drug therapy.

Mps1-catalyzed phosphorylation is microtubule-sensitive and counteracted by PP2A-B56 phosphatases to allow stable bipolar attachment

We next sought to determine which of the *in vivo* regulated phosphoproteins are direct substrates of Mps1. Previous studies have described Mps1's substantial but not strict preference for acid or amide side chains (i.e., D/E/N/Q) in the-3 and/or-2 positions (Dou et al., 2011; Hennrich et al., 2013). Consistently, 50% of the Mps1-regulated sites (14/28) exhibited this preference, rising to 70% (20/28) when substitution by an appropriately spaced phosphoserine or phosphothreonine was allowed (Table S1). Because these sites also fit the consensus for Plk1 (D/E/N/Q-X-S/T) (Alexander et al., 2011), we cross-referenced our data against recent phosphoproteomics studies with Plk1 inhibitors (Grosstessner-Hain et al., 2011; Kettenbach et al., 2011; Oppermann et al., 2012; Santamaria et al., 2011). Little overlap in regulation was observed, as 90% (19/21) of Mps1-dependent sites were unaffected by Plk1 inhibition (Table S1).

For further validation, we generated antibodies against two separate clusters of Mps1 autophosphorylation sites (pT33/pS37 and pT360/pS363), as well as the newly identified phosphosites in KNL1 (pS1831/pS1834), Rod (pT13/pS15), and Ska3 (pS34). Using these reagents, we verified each substrate's direct and site-specific phosphorylation by Mps1 *in vitro* (Fig. S3A), as well its dependence on Mps1 (but not Plk1) activity *in vivo* (Fig. 3A–C). We also examined Mps1-dependent phosphorylation at individual kinetochores by IFM, taking advantage of spindle poisons that block microtubule attachment (nocodazole) or permit attachment but not tension across kinetochores (monastrol). While Mps1 was recruited to unattached and tensionless kinetochores with similar efficiency, its auto-phosphorylation and trans-phosphorylation of substrates were significantly higher at the former (Fig. 3D–G). Graded microtubule-sensitive phosphorylation is a hallmark of dynamic error correction and SAC signaling pathways (Welburn et al., 2010) and typically depends on counteracting protein phosphatases (Foley et al., 2011; Liu et al., 2010; London et al., 2012; Rosenberg et al., 2011). As Mps1 indirectly recruits PP2A-B56 to kinetochores (Kruse et al., 2013; Suijkerbuijk et al., 2012), this phosphatase seemed particularly well suited to protect kinetochore-microtubule attachments from Mps1-induced turnover, in addition to promoting checkpoint reversal and re-activation of APC/C-Cdc20 (Espert et al., 2014; Kruse et al., 2013; Nijenhuis et al., 2014). Consistently, cells depleted of all PP2A-B56 isoforms exhibited high levels of Mps1-dependent phosphorylation at prometaphase kinetochores (Fig. 4A–B). Conversely, treating these cells with low levels of reversine led to almost complete restoration of cold-stable K-fibers (Fig. 4C–D). These results support and

extend our kinetochore-targeting experiments (Fig. 1) by demonstrating that endogenous Mps1 kinase activity is sufficient to disrupt K-fibers unless held in check by PP2A-B56.

Mps1 destabilizes the kinetochore-microtubule interface and promotes error correction by phosphorylating the hinge region of the Ska complex

Next we sought to identify specific substrates of Mps1 that mediate stable kinetochore-microtubule attachment only when unphosphorylated. During the examination of various candidates, we noticed that the Mps1-regulated phosphorylation site on Ska3 (S34) sits at the hinge of the W-shaped Ska complex (Fig. 5A). Because the hinge is organized by flanking ion-pair interactions (Jeyaprakash et al., 2012) and orients Ska1's distal microtubule-binding domains (Abad et al., 2014; Schmidt et al., 2012), we hypothesized that its phosphorylation could alter the Ska complex's association with kinetochores or interaction with microtubules. To test these possibilities we expressed wildtype (wt), unphosphorylatable (S34A), and phosphomimetic (S34D) forms of Ska3 as LAP-tagged fusions, and then depleted endogenous Ska3 with a 3′ UTR-specific siRNA (Fig. 5B). All three versions bound Ska1 and localized at kinetochores (Fig. 5C–D; see also Fig. 6F), indicating that Mps1-dependent phosphorylation on S34 does not control the Ska complex's recruitment by the KMN network, unlike Aurora B (Chan et al., 2012). However, cold-stability assays revealed a severe allele-specific defect in K-fiber integrity in Ska3^{S34D}-reconstituted cells (Fig. 5E–F).

To confirm and extend this result, timelapse microscopy was used to monitor the kinetics and accuracy of chromosome segregation. As expected (Gaitanos et al., 2009) Ska3 depletion impeded chromosome alignment, resulting in a prometaphase delay followed by cell death or aberrant anaphases with lagging chromosomes (Fig. 6A, rows 1–2, and Fig. 6B–C). In sharp contrast to the wildtype protein, neither Ska3^{S34D} nor Ska3^{S34A} rescued these mitotic defects (Fig. 6A, rows 3–5 and Fig. 6B–C), implying that both phosphorylation and dephosphorylation of this site are important for bi-orientation. We also used monastrol to generate large numbers of mal-oriented chromosomes, which then undergo error correction upon drug washout (Fig. 6D, upper panel). Loss of dynamic phosphorylation at S34 significantly reduced the efficiency of this process, as reflected in the persistence of mal-oriented chromosomes near the spindle poles (Fig. 6D, lower panel, and Fig. 6E). Both mutations also decreased tension at metaphase, as reflected in decreased separation of sister kinetochores (Fig. 6F–G). Together these data define the Ska complex as a physiologically relevant target of Mps1 at the kinetochore-microtubule interface, as phosphorylation of its hinge regulates attachment stability, tension generation, and correction of orientation errors.

Phosphomimetic hinge mutation reduces the Ska complex's microtubule residency time and impedes its lattice-to-end conversion during depolymerization

To understand these cell-based phenotypes, we asked how hinge phosphorylation affects the biochemical and biophysical properties of the Ska complex. As a first step, Ska1/Ska2/Ska3 (SKA^{wt}) and Ska1/Ska2/Ska3^{S34D} (SKA^{S34D}) complexes were purified from *Escherichia coli* (Fig. S4A). Size-exclusion chromatography and velocity sedimentation showed that both versions exist as dimers-of-trimers in solution (Fig. S4B–C), excluding a defect in holocomplex assembly. We also purified SKA^{wt}, SKA^{S34D}, and SKA^{S34A} tagged with GFP,

allowing interactions with the microtubule lattice and dynamic plus ends to be investigated using TIRF (total internal reflection fluorescence) microscopy. GFP-tagged SKA complexes bound both taxol-stabilized microtubules and vinblastine curls in co-pelleting assays (Fig. S4E–F), confirming their ability to recognize both straight and curved protofilaments (Schmidt et al., 2012). When reconstituted on GMP-CPP stabilized microtubules, each complex formed particles with the same average fluorescence intensity (Fig. S4G) and stepwise photobleaching behavior (Fig. S4H), indicating the presence of two GFP-Ska1 subunits (Schmidt et al., 2012). All complexes underwent 1-D diffusion along the microtubule lattice (Fig. 7A); however the SKA^{S34D} complex dissociated more quickly than SKA^{wt} or SKA^{S34A}, reducing its median residency time (Fig. 7B).

The Ska complex also binds and tracks depolymerizing plus ends autonomously (Schmidt et al., 2012). We therefore examined the behavior of each GFP-tagged complex on dynamic X-rhodamine-labeled microtubules (Fig. 7C–D). In all instances, an equivalent fraction of particles switched from lattice diffusion to processive tracking of shrinking (but not growing) microtubule ends (Fig. 7C–D and Fig. S4I). However, quantification revealed that end-tracking SKA^{S34D} particles were substantially dimmer than SKA^{wt} and SKA^{S34A} particles (Fig. 7E, left panel, and Fig. 7F). Because all three variants had similar fluorescence intensities during lattice diffusion (Fig. S4G), this observation suggests that SKA^{S34D} end-tracking particles contain fewer copies of the complex than normal. In principle this could reflect SKA^{S34D}'s shorter residency time, which would decrease its lattice density when combined with a low microtubule on-rate. However the lattice densities of SKA^{wt} and SKA^{S34D} complexes were equal at the relatively high protein concentration (10 nM) used in our end-tracking assays (Fig. S4I). This suggests that SKA^{S34D} complexes are lost specifically during lattice-to-end conversion. To address this issue, we compared the Ska complex's association with plus ends before and after a conversion event (Fig. 7E, right panel). Whereas SKA^{wt} and SKA^{S34A} were efficiently retained (median ratios of 1.01 and 0.99, respectively), on average one-third of SKA^{S34D} complexes were lost (Fig. 7G). These results suggest that hinge phosphorylation not only accelerates the Ska complex's turnover on the microtubule lattice, but also impedes its conversion into end-tracking complexes during microtubule depolymerization.

DISCUSSION

To ensure genome stability, eukaryotes delay anaphase until all sister chromatids are linked to the ends of microtubules from opposite poles, a configuration that generates tension and couples chromosome movement to microtubule dynamics (Foley and Kapoor, 2013). Successful bi-orientation requires not only efficient spindle assembly and kinetochore capture, but also selective correction of improper attachments. While error correction has been extensively studied as an Aurora B-specific phenomenon (Lampson and Cheeseman, 2011; Tanaka, 2010), it also requires Mps1, albeit for unknown reasons (Hewitt et al., 2010; Maciejowski et al., 2010; Maure et al., 2007; Santaguida et al., 2010). Here we provide evidence of an attachment-destabilizing activity that is intrinsic to Mps1 and epistatic to Aurora B. As a consequence of this activity, the formation and maintenance of stable attachments requires downregulation of Mps1-dependent phosphorylation by PP2A-B56 phosphatases and eviction of Mps1 from kinetochores. Through global phosphoproteomics,

we identified several new sites of Mps1-regulated phosphorylation at the outer kinetochore, including on the hinge region of the Ska complex, which binds and tracks depolymerizing microtubules and cooperates with the Ndc80 complex to mediate robust end-on attachment (Schmidt et al., 2012; Welburn et al., 2009). *In vivo* studies demonstrated the importance of reversible hinge phosphorylation for chromosome alignment and error correction, as well as defects in stable kinetochore-microtubule attachment that were specific to the phosphomimetic form of the Ska complex. *In vitro* reconstitution studies demonstrated that this form of the Ska complex also dissociates from the microtubule lattice more rapidly, and is impaired in conversion from lattice diffusion to end tracking during microtubule disassembly. These effects are at least partially separable, based on our assessment of the Ska complex's binding to plus ends before and after a conversion event. Given the complex's W-shaped structure, hinge phosphorylation might induce a conformational change that prevents multiple Ska complexes from coalescing into a larger end-tracking assembly. In this regard, we note that oligomerization of the yeast Dam1 complex is required for chromosome bi-orientation and requires a C-terminal domain in Dam1 that is a key target of Ipl1 (Aurora kinase) (Lampert et al., 2010; Tien et al., 2010; Umbreit et al., 2014; Zelter et al., 2015). As with Ska3, phosphomimetic and unphosphorylatable Dam1 mutants elicit high rates of chromosome missegregation, due to excessive (*dam1-4D*) or inadequate (*dam1-4A*) turnover of kinetochore-microtubule attachments (Kalantzaki et al., 2015). Thus, despite their divergent evolution, metazoan and fungal kinetochores may use the same basic principle (phosphorylation-sensitive oligomerization of microtubule end-tracking complexes) to drive the selective stabilization of bipolar attachments. Although not evident in our TIRF imaging assays, phosphorylation of the Ska complex hinge may also affect microtubule tip dynamics, as was noted for purified kinetochore particles from *dam1-4D* mutants (Sarangapani et al., 2013).

In cells, phosphorylation of Ska3 and other Mps1 substrates was high at unattached kinetochores but decreased as microtubule attachments formed and generated tension. While PP2A-B56 phosphatases counteract Mps1 during early mitosis, complete dephosphorylation of Mps1 substrates did not occur until metaphase, when Mps1 itself was evicted from kinetochores by microtubule occupancy and saturation of potential Mps1-docking sites within the Ndc80 complex (Hiruma et al., 2015; Ji et al., 2015). In addition to silencing the SAC, Mps1 eviction stabilizes kinetochore-microtubule attachments by dissipating inhibitory phosphorylation on Ska3 and other substrates, thus perpetuating Mps1's exclusion from kinetochores. While Aurora B-mediated phosphorylation also declines at metaphase, this is thought to be a primary consequence of tension across sister kinetochores (Lampson and Cheeseman, 2011; Tanaka, 2010). Consistent with the idea that two kinases sense and stabilize bi-orientation in parallel, targeting Mps1 to metaphase kinetochores disrupted K-fibers even when Aurora B was inhibited (Fig. 1D–E). This role of Mps1 may have escaped detection in previous studies due to less efficient tethering and activation of the kinase at kinetochores (Jelluma et al., 2010).

In addition to the Ska complex, Mps1-dependent phosphorylation was observed on other kinetochore modules involved in microtubule attachment, chromosome motility, and checkpoint signaling (Fig. 2D), providing numerous opportunities for functional, mechanistic, and evolutionary studies. In this regard, it is interesting that Mps1

phosphorylates the N-terminus of Rod, a subunit of the heterotrimeric RZZ complex that also shares homology with nucleoporins and other membrane-coating proteins (Civril et al., 2010). The widespread conservation of Rod orthologs in non-fungal eukaryotes (Schmitt, 2010) and recent evidence implicating nuclear pores as alternative scaffolds for MCC assembly (Rodriguez-Bravo et al., 2014) suggest that the SAC may have evolved from an earlier endomembrane-associated network (Schmitt, 2010; Wilson and Dawson, 2011). Conversely, the natural loss of the RZZ complex in fungi may explain their strict dependence on MELT motif phosphorylation for SAC function (London et al., 2012; Shepperd et al., 2012; Yamagishi et al., 2012), whereas this may be partially compensated by other Mps1 substrates in higher organisms (Krenn et al., 2014; Silio et al., 2015; Vleugel et al., 2013). Future studies will address how combinatorial phosphorylation of KNL1, Rod, and other Mps1 targets leads to a sensitive and robust checkpoint, as well as the mechanisms that govern their hierarchical recruitment and activation at kinetochores.

STAR ★ METHODS

CONTACT FOR REAGENT AND RESOURCE SHARING

Further information and requests for resources and reagents should be directed to and will be fulfilled by the Lead Contact, Prasad Jallepalli (jallepap@mskcc.org).

EXPERIMENTAL MODEL AND SUBJECT DETAILS

Cell lines used in this study are described in the Key Resources Table. HeLa cells (human cervical adenocarcinoma, female) were grown at 37°C in Dulbecco's modified eagle medium (DMEM) with 10% tetracycline free fetal bovine serum, 100 U/ml penicillin, and 100 U/ml streptomycin. Telomerase-immortalized RPE1 cells (human retinal pigment epithelium, female) were grown at 37°C in a 1:1 mixture of DMEM and Ham's F-12 medium with 10% fetal bovine serum, 100 U/ml penicillin, and 100 U/ml streptomycin, and 2.5 mM L-glutamine. Sf9 cells (Spodoptera frugiperda ovary, female) were grown at 27°C in Grace's insect medium with 10% fetal bovine serum, 100 U/ml penicillin, and 100 U/ml streptomycin.

METHOD DETAILS

Cell culture, plasmid and siRNA transfection, and chemical treatments—To express LAP-Mps1, LAP-Ska3, and GFP-Rod, pcDNA5/FRT/TO-based constructs were cotransfected with pOG44 into HeLa T-Rex Flp-In cells using FuGene 6 (Roche). Correct site-specific integrants were selected on the basis of hygromycin resistance and induced with tetracycline (Hewitt et al., 2010). FRB-mCherry-Mps1 was integrated into HeLa cells expressing Mis12-GFP-3xFKBP using recombinase-mediated cassette exchange (Ballister et al., 2014). Synthetic siRNAs were transfected into HeLa cells using Oligofectamine (ThermoFisher) and into hTERT-RPE1 cells using RNAiMax (ThermoFisher). For siRNA target sequences, see the Key Resources Table. Where indicated, 200 ng/ml nocodazole, 100 μM monastrol, 10 μM 3MB-PP1, 10 μM MG132, 500 nM rapamycin, 200–500 nM reversine, 10 μM Mps1-IN-1, 200 nM BI2536, 10 μM taxol, or 2 μM ZM447439 were added.

SILAC methods

Amino acid labeling and cell culture treatments: Mps1^{wt} and Mps1^{as} cells were grown in DMEM:F12 medium with 10% dialyzed fetal bovine serum and either 175 μM unlabeled L-arginine (Arg^{0}) and 250 μM unlabeled L-lysine (Lys^{0}) or the same concentrations of L-[U-$^{13}C_6$, $^{15}N_4$]-arginine (Arg^{10}) and L-[U-$^{13}C_6$, $^{15}N_2$]-lysine (Lys^{8}). After six cell doublings, 1.6 ×10^{6} cells were seeded per 15-cm dish (6 per experiment). 18 h later, 1 μg/ml aphidicolin was added for 12 h to synchronize cells in early S phase. Cells were then washed with PBS and cultured for another 13 h in fresh SILAC medium containing 50 ng/ml nocodazole to arrest cells in M phase. Thereafter the Arg^{0}Lys^{0}-labeled cells were treated with 10 μM MG132 and 5 μg/ml 3MB-PP1 (Burkard et al., 2007; Maciejowski et al., 2010), while the Arg^{10}Lys^{8}-labeled cells were treated with 10 μM MG132 alone. All cultures were harvested 2 hours later. This labeling scheme was used for first two replicates of each cell line and reversed for the last two replicates.

Sample preparation and mass spectrometry: After lysis in denaturing buffer (8 M urea, 50 mM Tris-HCl pH 8.2, 75 mM NaCl plus protease and phosphatase inhibitors), cell extracts were pooled, reduced, alkylated, and digested with endoproteinase Lys-C and trypsin (Daub et al., 2008). Peptides were filtered through a 0.22 μm PVDF membrane and desalted on reversed-phase C18 SepPak cartridges (Villen and Gygi, 2008), then snap-frozen in liquid nitrogen, lyophilized, and stored at −20°C. Peptides were dissolved in 600 μl of 7 mM KH2PO4 pH 2.65, 30% acetonitrile (ACN) and loaded onto a 250 × 9.4 mm polySULFOETHYL A column (PolyLC) operated with an ÄKTA explorer system (GE Healthcare) at 3 ml/min. The flow-through was collected and bound peptides were fractionated by a 30 min gradient ranging from 0% to 30% elution buffer (7 mM KH2PO4 pH of 2.65, 30% ACN, 350 mM KCl). SCX-separated fractions (3 ml) were pooled based on UV absorption (215 nm) to yield twelve samples with similar peptide amounts. For phosphopeptide enrichment, samples were lyophilized and resuspended in 200 μl of 25 mM formic acid, 40% acetonitrile, then incubated with 2.5 μl PHOS-Select Iron Affinity Gel (Sigma) for 1 hr at 25°C under continuous agitation. Phosphopeptides were eluted and desalted with C18 StageTips (Rappsilber et al., 2007; Villen and Gygi, 2008). In total 96 phosphopeptide samples were prepared and analyzed in technical replicates by LC-MS on a LTQ Orbitrap (Thermo Fisher Scientific) connected to a nanoflow HPLC system (Agilent 1100) via a nanoelectrospray ion source (Proxeon Biosystems).

Data processing and statistical analysis: All raw files acquired in this study were collectively processed with the MaxQuant software suite (version 1.0.13.13), which performs peak list generation, SILAC-based quantification, estimation of false discovery rates, peptide to protein group assembly, and phosphorylation site localization (Cox and Mann, 2008; Oppermann et al., 2012). Peak lists were searched against concatenated forward and reversed version of the human International Protein Index database (IPI version 3.37) using the Mascot search engine (version 2.2.04). SILAC spectra detected by pre-search MaxQuant analysis were searched with the additional fixed modifications Arg^{10} and/or Lys^{8}, whereas spectra for which a SILAC state was not assignable were searched with Arg^{10} and Lys^{8} as variable modifications. The accepted estimated FDR determined on the basis of peptide-spectral matches in the reversed database version was set to 1% for both peptide and

protein identifications. Phosphorylation sites were assigned by the PTM scoring algorithm implemented in MaxQuant (Olsen et al., 2006; Olsen et al., 2010). All phosphopeptide or phosphosite ratios measured in at least two biological replicates of each cell line were $\log_2$-transformed and subjected to two-class, unpaired SAM analysis of Mps1 as *versus* $Mps1^{wt}$ cells ± 3MB-PP1 (Oppermann et al., 2012; Tusher et al., 2001). Phosphopeptides and phosphosites of the SAM output with a false discovery rate (FDR or q value) of 0% (obtained for $\Delta \geq 1.189$ and $\Delta \geq 1.268$, respectively) and ≥ 2-fold regulation in 3MB-PP1-treated $Mps1^{as}$ cells were rated as significant.

Gene ontology and STRING network annotations—Mps1-regulated phosphoproteins (q-value = 0) were used to query the Gene Ontology Consortium database (Consortium, 2015). Significantly enriched annotation terms were identified using Fisher's exact test and *post hoc* correction using the Benjamini-Hochberg FDR. Network analysis was performed using proteome-wide interaction data from the STRING database (Szklarczyk et al., 2011) and curated using known spindle, kinetochore, and SAC signaling complexes (Cheeseman, 2014; London and Biggins, 2014).

Production of phosphospecific antibodies—To generate phosphospecific antibodies, peptides were synthesized at 90% purity and verified by reverse-phase HPLC and mass spectrometry (EZBiolab, Carmel, IN). 3 mg of each phosphopeptide was coupled to maleimide-activated keyhole limpet hemocyanin (Pierce) and injected into New Zealand White rabbits using an institutionally approved protocol and animal-care facility (Pocono Rabbit Farms and Laboratory, Canadensis, PA). Antisera were diluted 1:1 with TBS and loaded onto phosphopeptide-coupled Sulfolink columns (Pierce). After washing with TBS, high-salt buffer (20 mM Tris, pH 7.4, 0.5 M NaCl, 0.2% Triton X-100) and TBS, bound antibodies were eluted with 0.2 M glycine, pH 2.5, 150 mM NaCl, neutralized with 0.1 volume of 1 M Tris, pH 8.8, and loaded onto unphosphorylated peptide columns. Flowthrough fractions were assayed for phosphospecific reactivity by ELISA, adjusted to 25% glycerol, and stored at −80°C.

Peptide sequences and all antibodies used in this study are listed in the Key Resources Table.

Immunofluorescence microscopy—Cells were fixed and permeabilized via a 10-minute incubation in PEMFT (20 mM PIPES, pH 6.8, 10 mM EGTA, 1 mM $MgCl_2$, 4% paraformaldehyde, and 0.2% Triton X-100; Fig. 3G) or pre-extracted at 37°C for 90 seconds in PEMGT (100 mM PIPES pH 6.9, 10 mM EGTA, 1 mM $MgCl_2$, 4 M glycerol, and 0.5% Triton X-100) before incubating for 10 minutes in form-fix (3.7% formaldehyde and 0.2% Triton X-100 in PEMGT) (Fig. 1F, 3F, 4A, 4H, and 5D). For assessment of cold-stable microtubules, cells were held on ice in L-15 medium (ThermoFisher) for 10 min before incubating in form-fix for 10 min at room temperature. Specimens were blocked and stained with primary antibodies in 2% BSA or 10% goat serum, washed in TBS + 0.1% Triton X-100, and then stained with Alexa 488-, Alexa 561-, and/or Alexa 647-coupled secondary antibodies (ThermoFisher). Cells were counterstained with DAPI and mounted in Prolong Gold (ThermoFisher) prior to imaging.

For Fig. 1B and Fig. S1C, cells were imaged on a Leica DM6000 scanning confocal microscope with a 63x 1.4 NA objective and operated with Leica LASX software. Z-stacks were acquired with 0.3 μm spacing. For all other IFM, cells were imaged on a DeltaVision Image Restoration System (GE Healthcare) based on an Olympus IX-70 microscope with a 100x 1.4 NA oil objective and a CoolSnap QE cooled CCD camera (Photometrics). Z-stacks were acquired with 0.2 μm spacing, deconvolved using measured point spread functions, and displayed as maximum-intensity projections using SoftWorX. Fluorescence intensity measurements and background subtraction were performed with ImageJ. Images were cropped and assembled into figures using Photoshop CS4 (Adobe).

Live-cell imaging—For Fig. 1D and Fig. S1A, cells on poly-D-lysine coated coverslips were placed in a magnetic holder (Chamlide CM-S22-1, LCI) and mounted on a Leica DM4000 microscope equipped with a 100x 1.4 NA oil objective, piezo stage (ASI), spinning disk confocal head (Yokogawa), EMCCD camera (Hamamatsu), 488- and 593-nm laser lines, and environmental enclosure (PeCon GmBH). Each position was imaged over a 4 micron z-depth (5 slices, 1 μm/slice) in both fluorescence channels at every timepoint, and in DIC at the first and last timepoints. For Fig. 6A, cells were grown in 35 mm glass-bottom dishes (MatTek) and imaged on a Zeiss Axiovert 200 microscope fitted with a 63x 1.4 NA objective, piezo stage (Prior), spinning disk confocal head (Perkin-Elmer), EMCCD camera (Andor), 488- and 561-nm laser lines, and temperature-controlled stage enclosure with CO_2 support (Solent Scientific). Both systems were controlled by MetaMorph (Molecular Devices). Widefield timelapse imaging was performed on a Nikon TE2000 microscope equipped with 10x, 20x, and 40x air objectives, cooled CCD camera (Hamamatsu), temperature-controlled stage enclosure with CO_2 support (Solent Scientific), and NIS Elements software (Nikon).

Cell lysis, protein purification, and biochemical assays—Mammalian cell extracts were prepared by resuspending pellets in ice-cold buffer B (140 mM NaCl, 30 mM HEPES, pH 7.8, 5% glycerol, 10 mM sodium pyrophosphate, 5 mM sodium azide, 10 mM NaF, 10 mM PMSF, 0.3 mM sodium orthovanadate, 20 mM b-glycerophosphate, 1 mM DTT, 0.2 mM microcystin, and 1x protease inhibitor cocktail) prior to nitrogen cavitation (1250 psi, 45 min; Parr Instruments) and centrifugation at 20,000 x*g* for 30 min. LAP- and GFP-tagged proteins were precipitated using S protein-agarose or GFP antibody-Sepharose, resolved by SDS-PAGE, and transferred to PVDF membranes for Western blotting and detection via enhanced chemiluminescence.

To obtain active Mps1, baculovirus-infected Sf9 cells were lysed by sonication in insect cell breakage buffer (100 mM Tris, pH 7.5, 20% sucrose, 4 mM EDTA, and 0.01% NP-40). GST-Mps1 was retrieved on glutathione-agarose beads (GE Healthcare), washed extensively with wash buffer (100 mM Tris, pH 7.5, 20% sucrose, 4 mM EDTA, 500 mM KCl), and eluted in K buffer (20 mM potassium phosphate, pH 7.5, 10% glycerol, 0.5 mM EDTA, 0.5% NP-40, 25 mM glutathione, and 2 mM DTT). Eluted material was stored in single-use aliquots at −80°C. Separately, MBP-KNL1-C (1758–1862), GST-Rod-N (1–350) and GST-Ska3 were expressed in *E. coli* BL21 and purified on glutathione agarose or amylose resin (NEB). 6His-Ska1/Ska2 complexes were expressed in *E. coli* BL21 (DE3) and purified on

Ni-NTA agarose and Superose 200 chromatography (Schmidt et al., 2012; Welburn et al., 2009). 6His-Ska1/Ska2/Ska3 and 6His-GFP-Ska1/Ska2/Ska3 complexes were purified on glutathione agarose (via a PreScission protease-cleavable GST tag at the N-terminus of Ska3) and Superose 200 chromatography (Schmidt et al., 2012; Welburn et al., 2009). Analytical size-exclusion chromatography was performed on a Superose 6 column with 50 mM Tris, pH 7.4, 150 mM NaCl, 1 mM EDTA, 1 mM DTT as the mobile phase. For velocity sedimentation, samples were loaded onto a 5–20% sucrose gradient (in 25 mM Tris, pH 7.5, 0.01% NP-40, and 400 mM NaCl) and centrifuged at 250,000 x *g* for 24 hours at 4°C. Microtubule binding was assessed by loading protein complexes above a cushion of BRB80 (80 mM PIPES [pH 6.8], 1 mM EGTA, 1 mM $MgCl_2$) + 40% glycerol and centrifuging for 10 min at 80,000 x g (Schmidt et al., 2012; Welburn et al., 2009). Kinase assays were performed at 30°C for 30 to 60 minutes with 10 nM GST-Mps1 in 50 mM Tris-HCl, pH 7.5, 1 mM dithiothreitol, 10 mM $MgCl_2$, 10 mM β-glycerophosphate, 100 μM sodium orthovanadate, 100 μM ATP, and 500 nM substrate. Reactions were terminated with SDS-PAGE sample buffer and analyzed by Western blotting with phosphospecific or pan-reactive antibodies.

Imaging GFP-Ska complexes by total internal reflection microscopy (TIRF)— Flow chambers were assembled from sialylated coverslips and untreated glass slides using double-sided tape. For single-molecule assays, an antibody to β-tubulin were adsorbed onto the glass surface and the chamber blocked with 1% Pluronic F-127 (Sigma). GMP-CPP-stabilized microtubules labeled with HiLyte 647-tubulin (1:20) were allowed to bind to surface-bound antibodies and the chamber was perfused with 1 nM GFP-tagged Ska complex in assay buffer (80mM PIPES pH6.8, 1 mM $MgCl_2$, 1 mM EGTA), 50 mM KCl, 2 mM ATP, 0.1 mg/ml κ-casein, 80 μg/ml glucose, 40 μg/ml glucose-oxidase, 16 μg/ml catalase, 1 mM DTT). The chamber was sealed with VALAP (vaseline, lanolin, paraffin mixed 1:1:1) and imaged at 25°C on a Olympus CELLR/TIRF microscope (Olympus) equipped with a ImagEM emCCD camera (Hamamatsu Photonics), an environmental chamber and a stage-top-incubator (Okolab) using a 100x/1.49NA objective (Olympus) with 1.6x auxiliary magnification. To visualise the diffusive movement of Ska complexes, 90-second time-lapse videos were recorded at 10 frames per second (fps) using a 50 ms exposure to the 488 nm laser line. The position of the fixed microtubules was determined before and after the time-lapse video by capturing a single image using 640 nm laser lines (100 ms exposure). Kymographs were generated from line scans along microtubules and manually analyzed with ImageJ and the MultipleKymograph plugin (http://www.embl.de/eamnet/html/body_kymograph.html). For the analysis of microtubule residency time, only motile particles that associate and dissociate within the 90s window were considered. Intensity values of Ska complexes reflect the median intensity of the first 40 pixels of the intensity profile along the kymograph trace of the respective particle, corrected by local background subtraction. To determine bleaching steps of diffusing Ska complex particles, intensity profiles along kymograph traces were generated, corrected for local background, and manually fitted for constant intensity using Origin 9.1 (OriginLab).

For dynamic microtubule assays the glass surface was coated with poly-L-lysine-poly-ethylene-glycol-biotin (PLL-PEG-biotin, SurfaceSolutions), activated with 1 mg/ml

streptavidin and blocked with 1 mg/ml casein. Short GMP-CPP-stabilized microtubules (seeds) labeled 1:30 with biotin and HiLyte 647 were allowed to bind to the activated surface. The chamber was perfused with the assay mix (including 10 nM GFP-tagged Ska complex), which had been pre-cleared for 5 min in an Airfuge at 4°C and then sealed with VALAP. The assay mix contained 80 mM PIPES, pH 6.8, 4 mM $MgCl_2$, 1 mM EGTA, 1.3 mM GTP, 5.3 mM DTT, 67 mM glucose, 0.27 mg/ml catalase, 0.54 mg/ml glucose oxidase, 0.8 mg/ml κ-casein, 0.25% methyl cellulose, and a 1:10 mix of X-rhodamine-labeled and unlabeled tubulin. 5 min time-lapse movies were acquired at 35°C and one frame per second using the 488 nm and 561 nm laser lines at 150 ms and 100–150 ms exposure. The position of the fixed seeds was determined before and after every movement using the 640 nm laser line at 100 ms exposure. Intensity values of end-tracking Ska complexes reflect the median intensity of the first 10 pixels of the intensity profile along the kymograph trace of the respective particle, corrected by local background subtraction.

QUANTIFICATION AND STATISTICAL ANALYSIS

Details of quantitative and statistical analysis are provided in each figure legend and restated here. In Fig. 1B–C, integrated microtubule intensity was quantified in three experiments (n = 40 control and 57 rapamycin-treated cells) and compared using the Mann-Whitney U test. In Fig. 1D–E, The fraction of cells with no, low (≤ 4 affected chromosomes), medium (> 4 chromosomes), or high levels of misalignment (no discernable metaphase plate) was determined in five separate experiments (n = 90 to 180 cells per condition) and compared using two-way ANOVA and Sidak *post hoc* tests. In Fig. 1F–G, Dsn1 phosphorylation on serine 109 was quantified from ≥ 20 kinetochores of 10 cells per condition and compared using one-way ANOVA and Kruskal-Wallis *post hoc* tests. In Fig. 2C, enrichment of GO terms was analyzed using Fisher's exact test with correction using the Benjamini-Hochberg FDR. In Fig. 3G, fluorescence intensities were measured from 200 to 250 kinetochores per condition and compared using two-way ANOVA and Sidak *post hoc* tests. In Fig. 4A–B, fluorescence intensities were measured from 59 to 113 kinetochores per condition and compared using two-way ANOVA and Sidak *post hoc* tests. In Fig. 4C, the fraction of cells with few/no cold-stable microtubules was determined in three experiments (n ≥ 40 cells per condition per experiment) and compared using one-way ANOVA and Sidak *post hoc* tests. In Fig. 5E–F, cold-stable microtubules were quantified from 8 to 12 cells per condition in two experiments and compared using one-way ANOVA and Kruskal-Wallis *post hoc* test. In Fig. 6B, the length of M phase (from NEBD to mitotic exit or cell death) was quantified from 104 to 208 cells in three experiments and compared using one-way ANOVA and Kruskal-Wallis *post hoc* test. In Fig. 6D–E, chromosome alignment was determined from 40 to 100 cells per condition and compared using Fisher's exact test. In Fig. 6F–G, interkinetochore distances were measured from 105 to 130 sister kinetochore pairs (6 to 10 cells per condition) and compared using one-way ANOVA and Kruskal-Wallis *post hoc* test. In Fig. 7B, microtubule residency times were determined for SKA^{wt} (n=223), SKA^{S34A} (n=208), and SKA^{S34D} complexes (n=207) and compared using a Mann-Whitney U test. In Fig. 7F, median intensities of end-tracking SKA^{wt} (n=29), SKA^{S34A} (n=27), and SKA^{S34D} particles (n=19) were compared using a Mann-Whitney U test. In Fig. 7G, integrated post-conversion (ΣI_{post}) and pre-conversion (ΣI_{pre}) intensities were determined for SKA^{wt} (n=18),

SKA^{S34A} (n=14), and SKA^{S34D} particles (n=13) and compared using a Mann-Whitney U-test.

DATA AND SOFTWARE AVAILABILITY

Mass spectrometry proteomics data are available via the PRIDE archive (https://www.ebi.ac.uk/pride/archive/) under accession number PXD006135.

KEY RESOURCES TABLE

REAGENT or RESOURCE	SOURCE	IDENTIFIER
Antibodies		
pMps1-N rabbit polyclonal antibody (pT33/pS37)	this paper	N/A
pMps1-C rabbit polyclonal antibody (pT360/pS363)	this paper	N/A
pKNL1-C rabbit polyclonal antibody (pS1831/pS1834)	this paper	N/A
pSka3 rabbit polyclonal antibody (pS34)	this paper	N/A
mouse α-tubulin monoclonal antibody (clone DM1A) conjugated to FITC	Sigma	cat# F2168; RRID: AB_476967
rat α-tubulin monoclonal antibody (clone YL1/2)	AbD Serotec/Bio-Rad	cat# MCA77G; RRID: AB_325003
mouse β-tubulin monoclonal antibody (clone TUB2.1)	Sigma	cat #T5201; RRID: AB_609915
CREST auto-immune antibodies (human)	Immunovision	cat# HCT-0100
pDsn1 rabbit polyclonal antibody (pS109)	Iain Cheeseman (Welburn et al., 2010)	N/A
EGFP mouse monoclonal antibody (clone 3E6)	ThermoFisher	cat# A-11120; RRID: AB_221568
KNL1/CASC5 rabbit polyclonal antibody	Bethyl	cat# A300-805A; RRID: AB_2068711
Mps1/TTK rabbit polyclonal antibody	Santa Cruz	cat# sc-540; RRID: AB_632567
Ndc80/HEC1 mouse monoclonal antibody (clone 9G3)	Abcam	cat# ab3613; RRID:AB_303949
Rod/KNTC1 mouse monoclonal antibody	Santa Cruz	cat# sc-81853; RRID: AB_2133542
Ska1/C18orf24 rabbit polyclonal antibody	GeneTex	cat# GTX-119803; RRID: AB_10617818
Ska3 rabbit polyclonal antibody	Bethyl	cat# A304-215; RRID: AB_2620412
Bacterial and Virus Strains		
E. coli BL21	EMD Millipore	cat# 69449
E. coli BL21 (DE3)	EMD Millipore	cat# 69450
Biological Samples		
N/A		
Chemicals, Peptides, and Recombinant Proteins		

REAGENT or RESOURCE	SOURCE	IDENTIFIER
rapamycin	Sigma	cat# R0935; CAS Number: 53123-88-9
nocodazole	Sigma	cat# M1404; CAS Number: 31430-18-9
monastrol	Calbiochem	cat# 475879; CAS Number 254753-54- 3
taxol (paclitaxel)	Sigma	cat# T7402; CAS Number 33069-62-4
3-MB-PP1	Kevan Shokat (Burkard et al., 2007)	CAS Number 956025-83-5
MG132	Cayman Chemical	cat# 10012628; CAS Number 33407-82-6
reversine	Cayman Chemical	cat# 10004412; CAS Number 656820-32- 5
Mps1-IN-1	Nathanael Gray (Kwiatkowski et al., 2010)	CAS Number 1125593-20-5
BI-2536	MSKCC Organic Synthesis Core	CAS Number 755038-02-9
ZM447439	Tocris	cat# 2458; CAS Number 331771-20- 1
pMps1-N peptide: CKNEDL(pT)DEL(pS)LNKISA	this paper	N/A
Mps1-N peptide: CKNEDLTDELSLNKISA	this paper	N/A
pMps1-C peptide: CLKNK(pT)ES(pS)LLAK	this paper	N/A
Mps1-C peptide: CLKNKTESSLLAK	this paper	N/A
pKNL1-C peptide: CDIDK(pS)AN(pS)VLIK	this paper	N/A
KNL1-C peptide: CDIDKpSANSVLIK	this paper	N/A
pSka3 peptide: CALDGEE(pS)DFEDY	this paper	N/A
Ska3 peptide: CALDGEESDFEDY	this paper	N/A
pRod-N peptide: LLTNDD(pT)G(pS)GYLSVGC	this paper	N/A
Rod-N peptide: LLTNDDTGSGYLSVGC	this paper	N/A
GST-Mps1	this paper	N/A
GST-Mps1 (kinase dead, D664A)	this paper	N/A
GST-Mps1 (T33A S37A)	this paper	N/A
GST-Ska3 (WT), PreScission-cleavable	this paper	N/A
GST-Ska3 (S34A), PreScission-cleavable	this paper	N/A
GST-Ska3 (S34D), PreScission-cleavable	this paper	N/A
PreScission (human rhinovirus 3C) protease	GE Healthcare	cat# 27-0843-01
MBP-KNL1-C (1758–1862)	this paper	N/A
GST-Rod-N (1–350)	this paper	N/A
6His-Ska1/Ska2	this paper	N/A
6His-Ska1/Ska2/Ska3 (WT)	this paper	N/A
6His-Ska1/Ska2/Ska3 (S34D)	this paper	N/A
6His-EGFP-Ska1/Ska2/Ska3 (WT)	this paper	N/A

REAGENT or RESOURCE	SOURCE	IDENTIFIER
6His-EGFP-Ska1/Ska2/Ska3 (S34A)	this paper	N/A
6His-EGFP-Ska1/Ska2/Ska3 (S34D)	this paper	N/A
GTP	Jena Bioscience	cat# NU-1012; CAS number 36051-31-7
GMP-CPP	Jena Bioscience	cat# NU-405S; CAS number 14997-54-7
tubulin (fluorescent HiLyte 647): porcine brain	Cytoskeleton	cat# TL670M
tubulin (X-rhodamine): bovine brain	Cytoskeleton	cat# TL620M
tubulin (biotin): porcine brain	Cytoskeleton	cat# T333P
tubulin (unlabeled): porcine brain	McAinsh Lab	N/A
Critical Commercial Assays		
N/A		
Deposited Data		
Mass spectrometry proteomics data	this paper	PRIDE: PXD006135
Experimental Models: Cell Lines		
hTERT-RPE (telomerase-immortalized human retinal pigment epithelial cells)	ATCC	ATCC CRL-4000
TTK (Mps1) conditional-knockout hTERT-RPE cells	Jallepalli Lab; Maciejowski et al., 2010	N/A
Mps1^{wt} cells (*TTK*-null + EGFP-Mps1-wt)	Jallepalli Lab; Maciejowski et al., 2010	N/A
Mps1^{as} cells (*TTK*-null + EGFP-Mps1-M602A)	Jallepalli Lab; Maciejowski et al., 2010	N/A
HeLa T-Rex Flp-In cells	Stephen Taylor; Hewitt et al., 2010	N/A
HeLa T-Rex Flp-In + LAP-Ska3 (WT) + H2B-RFP	this paper	N/A
HeLa T-Rex Flp-In + LAP-Ska3 (S34A) + H2B-RFP	this paper	N/A
HeLa T-Rex Flp-In + LAP-Ska3 (S34D) + H2B-RFP	this paper	N/A
HeLa T-Rex Flp-In + LAP-Mps1	this paper	N/A
HeLa T-Rex Flp-In + LAP-Mps1^{2A} (T33A S37A)	this paper	N/A
HeLa T-Rex Flp-In + GFP-Rod	this paper	N/A
HeLa T-Rex Flp-In + GFP-Rod^{2A} (T13A S15A)	this paper	N/A
HeLa + Mis12-GFP-3xFKBP	Lampson Lab; Ballister et al., 2014	N/A
HeLa + Mis12-GFP-3xFKBP + FRB-mCherry-Mps1	this paper	N/A
Sf9 insect cells	ATCC	ATCC CRL-1711
Experimental Models: Organisms/Strains		
N/A		

REAGENT or RESOURCE	SOURCE	IDENTIFIER
Oligonucleotides		
siGL2 (CGUACGCGGAAUACUUCGA)	Gaitanos et al., 2009	N/A
siSKA3 (3′ UTR; AGACAAACAUGAACAUUAA)	Gaitanos et al., 2009	N/A
ON-TARGETplus siRNA, non-targeting control #1	Dharmacon	cat# D-001810-01
siB56-α (UGAAUGAACUGGUUGAGUA)	Foley et al., 2011	N/A
siB56-β (GAACAAUGAGUAUAUCCUA)	Foley et al., 2011	N/A
siB56-γ (GGAAGAUGAACCAACGUUA)	Foley et al., 2011	N/A
siB56-δ (UGACUGAGCCGGUAAUUGU)	Foley et al., 2011	N/A
siB56-ε (GCACAGCUGGCAUAUUGUA)	Foley et al., 2011	N/A
siKNL1 (AAGAUCUGAUUAAGGAUCCACGAAA)	Kiyomitsu et al., 2007	N/A
Recombinant DNA		
pcDNA5/FRT/TO (vector for FRT site-specific integration and tetracycline-inducible expression)	ThermoFisher	cat# V6520-20
pOG44 (FLP recombinase)	ThermoFisher	cat# V6005-20
pcDNA5/FRT/TO-LAP-Mps1	this paper	N/A
pcDNA5/FRT/TO-LAP-Ska3 (WT)	this paper	N/A
pcDNA5/FRT/TO-LAP-Ska3 (S34A)	this paper	N/A
pcDNA5/FRT/TO-LAP-Ska3 (S34D)	this paper	N/A
pcDNA5/FRT/TO-GFP-Rod	this paper	N/A
pcDNA5/FRT/TO-GFP-Rod (T13A S15A)	this paper	N/A
pRSF-Duet-6His-Ska1/Ska2	this paper	N/A
pRSF-Duet-6His-EGFP-Ska1/Ska2	this paper	N/A
pGEX-6P1-Ska3 (WT)	Iain Cheeseman; Schmidt et al., 2012	N/A
pGEX-6P1-Ska3 (S34A)	this paper	N/A
pGEX-6P1-Ska3 (S34D)	this paper	N/A
Software and Algorithms		
MaxQuant	Cox and Mann, 2008	http://www.coxdocs.org/doku.php?id=maxquant:common:downlo
SAM (R package)	Tusher et al., 2001; Oppermann et al., 2012	https://github.com/MikeJSeo/SAM
GO enrichment analysis	Gene Ontology Consortium, 2015	http://www.geneontology.org
STRING network analysis	Szklarczyk et al., 2011	http://string-db.org/
Cytoscape	Shannon et al., 2003	http://www.cytoscape.org
Other		
N/A		

Supplementary Material

Refer to Web version on PubMed Central for supplementary material.

Acknowledgments

We thank Iain Cheeseman (Whitehead Institute), Nathanael Gray (Dana-Farber Cancer Institute), Kevan Shokat (UCSF), and Stephen Taylor (University of Manchester) for generous gifts of reagents and Alison North (Rockefeller University Bio-Imaging Resource Center) for assistance with spinning disk microscopy. P.V.J. was supported by grants from the National Institutes of Health (R01GM094972 and P30CA008748). A.D.M. was supported by a Wellcome Trust Senior Investigator Award [106151/Z/14/Z] and a Royal Society Wolfson Research Merit Award (WM150020).

References

Abad MA, Medina B, Santamaria A, Zou J, Plasberg-Hill C, Madhumalar A, Jayachandran U, Redli PM, Rappsilber J, Nigg EA, et al. Structural basis for microtubule recognition by the human kinetochore Ska complex. Nature communications. 2014; 5:2964.

Alexander J, Lim D, Joughin BA, Hegemann B, Hutchins JR, Ehrenberger T, Ivins F, Sessa F, Hudecz O, Nigg EA, et al. Spatial exclusivity combined with positive and negative selection of phosphorylation motifs is the basis for context-dependent mitotic signaling. Sci Signal. 2011; 4

Ballister ER, Riegman M, Lampson MA. Recruitment of Mad1 to metaphase kinetochores is sufficient to reactivate the mitotic checkpoint. J Cell Biol. 2014; 204:901–908. [PubMed: 24637323]

Barisic M, Sohm B, Mikolcevic P, Wandke C, Rauch V, Ringer T, Hess M, Bonn G, Geley S. Spindly/CCDC99 is required for efficient chromosome congression and mitotic checkpoint regulation. Molecular biology of the cell. 2010; 21:1968–1981. [PubMed: 20427577]

Buffin E, Lefebvre C, Huang J, Gagou ME, Karess RE. Recruitment of Mad2 to the kinetochore requires the Rod/Zw10 complex. Curr Biol. 2005; 15:856–861. [PubMed: 15886105]

Burkard ME, Randall CL, Larochelle S, Zhang C, Shokat KM, Fisher RP, Jallepalli PV. Chemical genetics reveals the requirement for Polo-like kinase 1 activity in positioning RhoA and triggering cytokinesis in human cells. Proc Natl Acad Sci USA. 2007; 104:4383–4388. [PubMed: 17360533]

Chan YW, Fava LL, Uldschmid A, Schmitz MH, Gerlich DW, Nigg EA, Santamaria A. Mitotic control of kinetochore-associated dynein and spindle orientation by human Spindly. J Cell Biol. 2009; 185:859–874. [PubMed: 19468067]

Chan YW, Jeyaprakash AA, Nigg EA, Santamaria A. Aurora B controls kinetochore-microtubule attachments by inhibiting Ska complex-KMN network interaction. J Cell Biol. 2012; 196:563–571. [PubMed: 22371557]

Cheeseman IM. The kinetochore. Cold Spring Harbor perspectives in biology. 2014; 6:a015826. [PubMed: 24984773]

Civril F, Wehenkel A, Giorgi FM, Santaguida S, Di Fonzo A, Grigorean G, Ciccarelli FD, Musacchio A. Structural analysis of the RZZ complex reveals common ancestry with multisubunit vesicle tethering machinery. Structure. 2010; 18:616–626. [PubMed: 20462495]

Consortium GO. Gene Ontology Consortium: going forward. Nucleic Acids Res. 2015; 43:D1049–1056. [PubMed: 25428369]

Cox J, Mann M. MaxQuant enables high peptide identification rates, individualized p.p.b.-range mass accuracies and proteome-wide protein quantification. Nature biotechnology. 2008; 26:1367–1372.

Daub H, Olsen JV, Bairlein M, Gnad F, Oppermann FS, Korner R, Greff Z, Keri G, Stemmann O, Mann M. Kinase-selective enrichment enables quantitative phosphoproteomics of the kinome across the cell cycle. Mol Cell. 2008; 31:438–448. [PubMed: 18691976]

Ditchfield C, Johnson VL, Tighe A, Ellston R, Haworth C, Johnson T, Mortlock A, Keen N, Taylor SS. Aurora B couples chromosome alignment with anaphase by targeting BubR1, Mad2, and Cenp-E to kinetochores. J Cell Biol. 2003; 161:267–280. [PubMed: 12719470]

Dou Z, von Schubert C, Korner R, Santamaria A, Elowe S, Nigg EA. Quantitative mass spectrometry analysis reveals similar substrate consensus motif for human Mps1 kinase and Plk1. PLoS One. 2011; 6:e18793. [PubMed: 21533207]

Espert A, Uluocak P, Bastos RN, Mangat D, Graab P, Gruneberg U. PP2A-B56 opposes Mps1 phosphorylation of Knl1 and thereby promotes spindle assembly checkpoint silencing. J Cell Biol. 2014; 206:833–842. [PubMed: 25246613]

Espeut J, Gaussen A, Bieling P, Morin V, Prieto S, Fesquet D, Surrey T, Abrieu A. Phosphorylation relieves autoinhibition of the kinetochore motor Cenp-E. Mol Cell. 2008; 29:637–643. [PubMed: 18342609]

Foley EA, Kapoor TM. Microtubule attachment and spindle assembly checkpoint signalling at the kinetochore. Nat Rev Mol Cell Biol. 2013; 14:25–37. [PubMed: 23258294]

Foley EA, Maldonado M, Kapoor TM. Formation of stable attachments between kinetochores and microtubules depends on the B56-PP2A phosphatase. Nat Cell Biol. 2011; 13:1265–1271. [PubMed: 21874008]

Gaitanos TN, Santamaria A, Jeyaprakash AA, Wang B, Conti E, Nigg EA. Stable kinetochore-microtubule interactions depend on the Ska complex and its new component Ska3/C13Orf3. EMBO J. 2009; 28:1442–1452. [PubMed: 19360002]

Gassmann R, Essex A, Hu JS, Maddox PS, Motegi F, Sugimoto A, O'Rourke SM, Bowerman B, McLeod I, Yates JR 3rd, et al. A new mechanism controlling kinetochore-microtubule interactions revealed by comparison of two dynein-targeting components: SPDL-1 and the Rod/Zwilch/Zw10 complex. Genes Dev. 2008; 22:2385–2399. [PubMed: 18765790]

Griffis ER, Stuurman N, Vale RD. Spindly, a novel protein essential for silencing the spindle assembly checkpoint, recruits dynein to the kinetochore. J Cell Biol. 2007; 177:1005–1015. [PubMed: 17576797]

Grosstessner-Hain K, Hegemann B, Novatchkova M, Rameseder J, Joughin BA, Hudecz O, Roitinger E, Pichler P, Kraut N, Yaffe MB, et al. Quantitative phospho-proteomics to investigate the polo-like kinase 1-dependent phospho-proteome. Mol Cell Proteomics. 2011; 10:M111 008540.

Gudimchuk N, Vitre B, Kim Y, Kiyatkin A, Cleveland DW, Ataullakhanov FI, Grishchuk EL. Kinetochore kinesin CENP-E is a processive bi-directional tracker of dynamic microtubule tips. Nat Cell Biol. 2013; 15:1079–1088. [PubMed: 23955301]

Hennrich ML, Marino F, Groenewold V, Kops GJ, Mohammed S, Heck AJ. Universal quantitative kinase assay based on diagonal SCX chromatography and stable isotope dimethyl labeling provides high-definition kinase consensus motifs for PKA and human Mps1. Journal of proteome research. 2013; 12:2214–2224. [PubMed: 23510141]

Hewitt L, Tighe A, Santaguida S, White AM, Jones CD, Musacchio A, Green S, Taylor SS. Sustained Mps1 activity is required in mitosis to recruit O-Mad2 to the Mad1-C-Mad2 core complex. J Cell Biol. 2010; 190:25–34. [PubMed: 20624899]

Hiruma Y, Sacristan C, Pachis ST, Adamopoulos A, Kuijt T, Ubbink M, von Castelmur E, Perrakis A, Kops GJ. Competition between MPS1 and microtubules at kinetochores regulates spindle checkpoint signaling. Science. 2015; 348:1264–1267. [PubMed: 26068855]

Howell BJ, Moree B, Farrar EM, Stewart S, Fang G, Salmon ED. Spindle checkpoint protein dynamics at kinetochores in living cells. Curr Biol. 2004; 14:953–964. [PubMed: 15182668]

Jelluma N, Brenkman AB, McLeod I, Yates JR 3rd, Cleveland DW, Medema RH, Kops GJ. Chromosomal instability by inefficient Mps1 auto-activation due to a weakened mitotic checkpoint and lagging chromosomes. PLoS One. 2008a; 3:e2415. [PubMed: 18545697]

Jelluma N, Brenkman AB, van den Broek NJ, Cruijsen CW, van Osch MH, Lens SM, Medema RH, Kops GJ. Mps1 phosphorylates Borealin to control Aurora B activity and chromosome alignment. Cell. 2008b; 132:233–246. [PubMed: 18243099]

Jelluma N, Dansen TB, Sliedrecht T, Kwiatkowski NP, Kops GJ. Release of Mps1 from kinetochores is crucial for timely anaphase onset. J Cell Biol. 2010; 191:281–290. [PubMed: 20937696]

Jeyaprakash AA, Santamaria A, Jayachandran U, Chan YW, Benda C, Nigg EA, Conti E. Structural and functional organization of the Ska complex, a key component of the kinetochore-microtubule interface. Mol Cell. 2012; 46:274–286. [PubMed: 22483620]

Ji Z, Gao H, Yu H. Kinetochore attachment sensed by competitive Mps1 and microtubule binding to Ndc80C. Science. 2015; 348:1260–1264. [PubMed: 26068854]

Kalantzaki M, Kitamura E, Zhang T, Mino A, Novak B, Tanaka TU. Kinetochore-microtubule error correction is driven by differentially regulated interaction modes. Nat Cell Biol. 2015; 17:421–433. [PubMed: 25751138]

Kang J, Chen Y, Zhao Y, Yu H. Autophosphorylation-dependent activation of human Mps1 is required for the spindle checkpoint. Proc Natl Acad Sci U S A. 2007; 104:20232–20237. [PubMed: 18083840]

Kawashima SA, Yamagishi Y, Honda T, Ishiguro K, Watanabe Y. Phosphorylation of H2A by Bub1 prevents chromosomal instability through localizing shugoshin. Science. 2010; 327:172–177. [PubMed: 19965387]

Kelly AE, Funabiki H. Correcting aberrant kinetochore microtubule attachments: an Aurora B-centric view. Curr Opin Cell Biol. 2009; 21:51–58. [PubMed: 19185479]

Kettenbach AN, Schweppe DK, Faherty BK, Pechenick D, Pletnev AA, Gerber SA. Quantitative phosphoproteomics identifies substrates and functional modules of Aurora and Polo-like kinase activities in mitotic cells. Sci Signal. 2011; 4:rs5. [PubMed: 21712546]

Kim Y, Heuser JE, Waterman CM, Cleveland DW. CENP-E combines a slow, processive motor and a flexible coiled coil to produce an essential motile kinetochore tether. J Cell Biol. 2008; 181:411–419. [PubMed: 18443223]

Kiyomitsu T, Obuse C, Yanagida M. Human Blinkin/AF15q14 is required for chromosome alignment and the mitotic checkpoint through direct interaction with Bub1 and BubR1. Dev Cell. 2007; 13:663–676. [PubMed: 17981135]

Kops GJ, Kim Y, Weaver BA, Mao Y, McLeod I, Yates JR 3rd, Tagaya M, Cleveland DW. ZW10 links mitotic checkpoint signaling to the structural kinetochore. J Cell Biol. 2005; 169:49–60. [PubMed: 15824131]

Krenn V, Overlack K, Primorac I, van Gerwen S, Musacchio A. KI motifs of human Knl1 enhance assembly of comprehensive spindle checkpoint complexes around MELT repeats. Curr Biol. 2014; 24:29–39. [PubMed: 24361068]

Kruse T, Zhang G, Larsen MS, Lischetti T, Streicher W, Kragh Nielsen T, Bjorn SP, Nilsson J. Direct binding between BubR1 and B56-PP2A phosphatase complexes regulate mitotic progression. J Cell Sci. 2013; 126:1086–1092. [PubMed: 23345399]

Kuijt TE, Omerzu M, Saurin AT, Kops GJ. Conditional targeting of MAD1 to kinetochores is sufficient to reactivate the spindle assembly checkpoint in metaphase. Chromosoma. 2014; 123:471–480. [PubMed: 24695965]

Kwiatkowski N, Jelluma N, Filippakopoulos P, Soundararajan M, Manak MS, Kwon M, Choi HG, Sim T, Deveraux QL, Rottmann S, et al. Small-molecule kinase inhibitors provide insight into Mps1 cell cycle function. Nature chemical biology. 2010; 6:359–368. [PubMed: 20383151]

Lampert F, Hornung P, Westermann S. The Dam1 complex confers microtubule plus end-tracking activity to the Ndc80 kinetochore complex. J Cell Biol. 2010; 189:641–649. [PubMed: 20479465]

Lampson MA, Cheeseman IM. Sensing centromere tension: Aurora B and the regulation of kinetochore function. Trends Cell Biol. 2011; 21:133–140. [PubMed: 21106376]

Lenart P, Petronczki M, Steegmaier M, Di Fiore B, Lipp JJ, Hoffmann M, Rettig WJ, Kraut N, Peters JM. The small-molecule inhibitor BI 2536 reveals novel insights into mitotic roles of polo-like kinase 1. Curr Biol. 2007; 17:304–315. [PubMed: 17291761]

Liu D, Vader G, Vromans M, Lampson M, Lens S. Sensing chromosome bi-orientation by spatial separation of aurora B kinase from kinetochore substrates. Science. 2009; 323:1350–1353. [PubMed: 19150808]

Liu D, Vleugel M, Backer CB, Hori T, Fukagawa T, Cheeseman IM, Lampson MA. Regulated targeting of protein phosphatase 1 to the outer kinetochore by KNL1 opposes Aurora B kinase. J Cell Biol. 2010; 188:809–820. [PubMed: 20231380]

London N, Biggins S. Signalling dynamics in the spindle checkpoint response. Nat Rev Mol Cell Biol. 2014; 15:736–747. [PubMed: 25303117]

London N, Ceto S, Ranish JA, Biggins S. Phosphoregulation of Spc105 by Mps1 and PP1 regulates Bub1 localization to kinetochores. Curr Biol. 2012; 22:900–906. [PubMed: 22521787]

Maciejowski J, George KA, Terret ME, Zhang C, Shokat KM, Jallepalli PV. Mps1 directs the assembly of Cdc20 inhibitory complexes during interphase and mitosis to control M phase timing and spindle checkpoint signaling. J Cell Biol. 2010; 190:89–100. [PubMed: 20624902]

Mattison CP, Old WM, Steiner E, Huneycutt BJ, Resing KA, Ahn NG, Winey M. Mps1 activation loop autophosphorylation enhances kinase activity. J Biol Chem. 2007; 282:30553–30561. [PubMed: 17728254]

Maure JF, Kitamura E, Tanaka TU. Mps1 kinase promotes sister-kinetochore bi-orientation by a tension-dependent mechanism. Curr Biol. 2007; 17:2175–2182. [PubMed: 18060784]

Nijenhuis W, Vallardi G, Teixeira A, Kops GJ, Saurin AT. Negative feedback at kinetochores underlies a responsive spindle checkpoint signal. Nat Cell Biol. 2014; 16:1257–1264. [PubMed: 25402682]

Nijenhuis W, von Castelmur E, Littler D, De Marco V, Tromer E, Vleugel M, van Osch MH, Snel B, Perrakis A, Kops GJ. A TPR domain-containing N-terminal module of MPS1 is required for its kinetochore localization by Aurora B. J Cell Biol. 2013; 201:217–231. [PubMed: 23569217]

Olsen JV, Blagoev B, Gnad F, Macek B, Kumar C, Mortensen P, Mann M. Global, in vivo, and site-specific phosphorylation dynamics in signaling networks. Cell. 2006; 127:635–648. [PubMed: 17081983]

Olsen JV, Vermeulen M, Santamaria A, Kumar C, Miller ML, Jensen LJ, Gnad F, Cox J, Jensen TS, Nigg EA, et al. Quantitative phosphoproteomics reveals widespread full phosphorylation site occupancy during mitosis. Sci Signal. 2010; 3:ra3. [PubMed: 20068231]

Oppermann FS, Grundner-Culemann K, Kumar C, Gruss OJ, Jallepalli PV, Daub H. Combination of chemical genetics and phosphoproteomics for kinase signaling analysis enables confident identification of cellular downstream targets. Mol Cell Proteomics. 2012; 11:O111 012351.

Raaijmakers JA, Tanenbaum ME, Maia AF, Medema RH. RAMA1 is a novel kinetochore protein involved in kinetochore-microtubule attachment. J Cell Sci. 2009; 122:2436–2445. [PubMed: 19549680]

Rappsilber J, Mann M, Ishihama Y. Protocol for micro-purification, enrichment, pre-fractionation and storage of peptides for proteomics using StageTips. Nature protocols. 2007; 2:1896–1906. [PubMed: 17703201]

Rieder CL. The structure of the cold-stable kinetochore fiber in metaphase PtK1 cells. Chromosoma. 1981; 84:145–158. [PubMed: 7297248]

Rodriguez-Bravo V, Maciejowski J, Corona J, Buch HK, Collin P, Kanemaki MT, Shah JV, Jallepalli PV. Nuclear pores protect genome integrity by assembling a premitotic and mad1-dependent anaphase inhibitor. Cell. 2014; 156:1017–1031. [PubMed: 24581499]

Rosenberg JS, Cross FR, Funabiki H. KNL1/Spc105 recruits PP1 to silence the spindle assembly checkpoint. Curr Biol. 2011; 21:942–947. [PubMed: 21640906]

Santaguida S, Tighe A, D'Alise AM, Taylor SS, Musacchio A. Dissecting the role of MPS1 in chromosome biorientation and the spindle checkpoint through the small molecule inhibitor reversine. J Cell Biol. 2010; 190:73–87. [PubMed: 20624901]

Santaguida S, Vernieri C, Villa F, Ciliberto A, Musacchio A. Evidence that Aurora B is implicated in spindle checkpoint signalling independently of error correction. EMBO J. 2011; 30:1508–1519. [PubMed: 21407176]

Santamaria A, Wang B, Elowe S, Malik R, Zhang F, Bauer M, Schmidt A, Sillje HH, Korner R, Nigg EA. The Plk1-dependent phosphoproteome of the early mitotic spindle. Mol Cell Proteomics. 2011; 10:M110 004457.

Sarangapani KK, Akiyoshi B, Duggan NM, Biggins S, Asbury CL. Phosphoregulation promotes release of kinetochores from dynamic microtubules via multiple mechanisms. Proc Natl Acad Sci U S A. 2013; 110:7282–7287. [PubMed: 23589891]

Saurin AT, van der Waal MS, Medema RH, Lens SM, Kops GJ. Aurora B potentiates Mps1 activation to ensure rapid checkpoint establishment at the onset of mitosis. Nature communications. 2011; 2:316.

Schmidt JC, Arthanari H, Boeszoermenyi A, Dashkevich NM, Wilson-Kubalek EM, Monnier N, Markus M, Oberer M, Milligan RA, Bathe M, et al. The kinetochore-bound Ska1 complex tracks depolymerizing microtubules and binds to curved protofilaments. Dev Cell. 2012; 23:968–980. [PubMed: 23085020]

Schmitt HD. Dsl1p/Zw10: common mechanisms behind tethering vesicles and microtubules. Trends Cell Biol. 2010; 20:257–268. [PubMed: 20226673]

Shannon P, Markiel A, Ozier O, Baliga NS, Wang JT, Ramage D, Amin N, Schwikowski B, Ideker T. Cytoscape: a software environment for integrated models of biomolecular interaction networks. Genome research. 2003; 13:2498–2504. [PubMed: 14597658]

Shepperd LA, Meadows JC, Sochaj AM, Lancaster TC, Zou J, Buttrick GJ, Rappsilber J, Hardwick KG, Millar JB. Phosphodependent recruitment of Bub1 and Bub3 to Spc7/KNL1 by Mph1 kinase maintains the spindle checkpoint. Curr Biol. 2012; 22:891–899. [PubMed: 22521786]

Shi J, Zhou Y, Huang HC, Mitchison TJ. Navitoclax (ABT-263) accelerates apoptosis during drug-induced mitotic arrest by antagonizing Bcl-xL. Cancer Res. 2011; 71:4518–4526. [PubMed: 21546570]

Silio V, McAinsh AD, Millar JB. KNL1-Bubs and RZZ Provide Two Separable Pathways for Checkpoint Activation at Human Kinetochores. Dev Cell. 2015; 35:600–613. [PubMed: 26651294]

Sliedrecht T, Zhang C, Shokat KM, Kops GJ. Chemical genetic inhibition of Mps1 in stable human cell lines reveals novel aspects of Mps1 function in mitosis. PLoS One. 2010; 5:e10251. [PubMed: 20422024]

Suijkerbuijk SJ, Vleugel M, Teixeira A, Kops GJ. Integration of kinase and phosphatase activities by BUBR1 ensures formation of stable kinetochore-microtubule attachments. Dev Cell. 2012; 23:745–755. [PubMed: 23079597]

Szklarczyk D, Franceschini A, Kuhn M, Simonovic M, Roth A, Minguez P, Doerks T, Stark M, Muller J, Bork P, et al. The STRING database in 2011: functional interaction networks of proteins, globally integrated and scored. Nucleic Acids Res. 2011; 39:D561–568. [PubMed: 21045058]

Tanaka TU. Kinetochore-microtubule interactions: steps towards bi-orientation. EMBO J. 2010; 29:4070–4082. [PubMed: 21102558]

Tien JF, Umbreit NT, Gestaut DR, Franck AD, Cooper J, Wordeman L, Gonen T, Asbury CL, Davis TN. Cooperation of the Dam1 and Ndc80 kinetochore complexes enhances microtubule coupling and is regulated by aurora B. J Cell Biol. 2010; 189:713–723. [PubMed: 20479468]

Tusher VG, Tibshirani R, Chu G. Significance analysis of microarrays applied to the ionizing radiation response. Proc Natl Acad Sci U S A. 2001; 98:5116–5121. [PubMed: 11309499]

Umbreit NT, Miller MP, Tien JF, Ortola JC, Gui L, Lee KK, Biggins S, Asbury CL, Davis TN. Kinetochores require oligomerization of Dam1 complex to maintain microtubule attachments against tension and promote biorientation. Nature communications. 2014; 5:4951.

Vergnolle MA, Taylor SS. Cenp-F links kinetochores to Ndel1/Nde1/Lis1/dynein microtubule motor complexes. Curr Biol. 2007; 17:1173–1179. [PubMed: 17600710]

Villen J, Gygi SP. The SCX/IMAC enrichment approach for global phosphorylation analysis by mass spectrometry. Nature protocols. 2008; 3:1630–1638. [PubMed: 18833199]

Vleugel M, Tromer E, Omerzu M, Groenewold V, Nijenhuis W, Snel B, Kops GJ. Arrayed BUB recruitment modules in the kinetochore scaffold KNL1 promote accurate chromosome segregation. J Cell Biol. 2013; 203:943–955. [PubMed: 24344183]

Welburn JP, Grishchuk EL, Backer CB, Wilson-Kubalek EM, Yates JR 3rd, Cheeseman IM. The human kinetochore Ska1 complex facilitates microtubule depolymerization-coupled motility. Dev Cell. 2009; 16:374–385. [PubMed: 19289083]

Welburn JP, Vleugel M, Liu D, Yates JR 3rd, Lampson MA, Fukagawa T, Cheeseman IM. Aurora B phosphorylates spatially distinct targets to differentially regulate the kinetochore-microtubule interface. Mol Cell. 2010; 38:383–392. [PubMed: 20471944]

Wilson KL, Dawson SC. Evolution: functional evolution of nuclear structure. J Cell Biol. 2011; 195:171–181. [PubMed: 22006947]

Xu P, Raetz EA, Kitagawa M, Virshup DM, Lee SH. BUBR1 recruits PP2A via the B56 family of targeting subunits to promote chromosome congression. Biology open. 2013; 2:479–486. [PubMed: 23789096]

Yamagishi Y, Yang CH, Tanno Y, Watanabe Y. MPS1/Mph1 phosphorylates the kinetochore protein KNL1/Spc7 to recruit SAC components. Nat Cell Biol. 2012; 14:746–752. [PubMed: 22660415]

Yang Z, Guo J, Chen Q, Ding C, Du J, Zhu X. Silencing mitosin induces misaligned chromosomes, premature chromosome decondensation before anaphase onset, and mitotic cell death. Molecular and cellular biology. 2005; 25:4062–4074. [PubMed: 15870278]

Zelter A, Bonomi M, Kim J, Umbreit NT, Hoopmann MR, Johnson R, Riffle M, Jaschob D, MacCoss MJ, Moritz RL, et al. The molecular architecture of the Dam1 kinetochore complex is defined by cross-linking based structural modelling. Nature communications. 2015; 6:8673.

Zhong Q, Gao W, Du F, Wang X. Mule/ARF-BP1, a BH3-only E3 ubiquitin ligase, catalyzes the polyubiquitination of Mcl-1 and regulates apoptosis. Cell. 2005; 121:1085–1095. [PubMed: 15989957]

Zich J, May K, Paraskevopoulos K, Sen O, Syred HM, van der Sar S, Patel H, Moresco JJ, Sarkeshik A, Yates JR 3rd, et al. Mps1Mph1 Kinase Phosphorylates Mad3 to Inhibit Cdc20Slp1-APC/C and Maintain Spindle Checkpoint Arrests. PLoS Genet. 2016; 12:e1005834. [PubMed: 26882497]

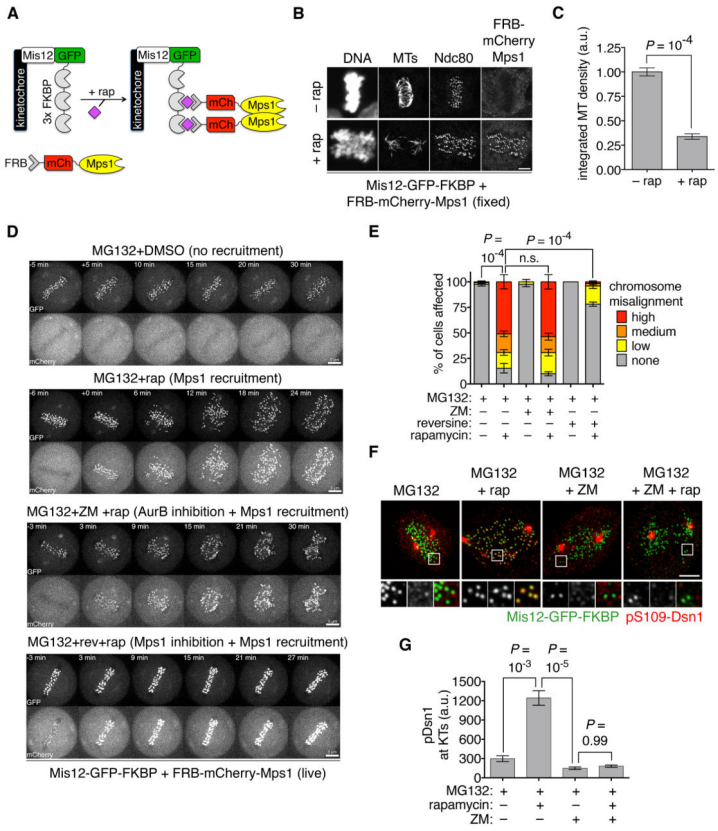

Figure 1. Kinetochore-associated Mps1 destabilizes microtubule attachment independently of Aurora B

(A) Strategy for chemically controlled targeting of Mps1 to metaphase kinetochores. FRB-mCherry-Mps1 was co-expressed with Mis12-GFP-FKBP in HeLa cells stably depleted of endogenous FKBP (Ballister et al., 2014). Kinetochore localization occurred within minutes of rapamycin addition (Fig. S1A). (B and C) Targeting Mps1 to kinetochores disrupts preformed K-fibers. Cells expressing FRB-mCherry-Mps1 and Mis12-GFP-FKBP were cultured with or without rapamycin for 20 minutes, then incubated on ice for 10 minutes prior to fixation and immunostaining as shown. Ndc80 was used to detect kinetochores. Integrated MT intensity was quantified in three separate experiments (n = 40 control and 57 rapamycin-treated cells) and compared using the Mann-Whitney U test. Error bars indicate SEM. Scale bars, 5 μm. (D and E) Kinetochore-targeted Mps1 disrupts metaphase bi-orientation independently of Aurora B. Cells expressing FRB-mCherry-Mps1 and Mis12-GFP-FKBP were cultured in MG132 for 20 minutes to induce metaphase arrest. Thereafter, cells were maintained in MG132 ± reversine (rev) or ZM447439 (ZM) for 60 minutes to pre-inhibit Mps1 or Aurora B, and then imaged during a final 30-min treatment with rapamycin or solvent (DMSO). The fraction of cells with no, low (≤ 4 affected chromosomes), medium (> 4 chromosomes), or high levels of misalignment (no discernable metaphase plate) was determined in five separate experiments (n = 90 to 180 cells per condition; representative images shown in panel D and Fig. S1D) and compared using two-way ANOVA and Sidak *post hoc* tests. Error bars indicate SEM. (F and G) Cells expressing FRB-mCherry-Mps1 and Mis12-GFP-FKBP were treated as in Fig. 1D, then fixed and stained with antibodies to

Aurora B-phosphorylated Dsn1 (pS109-Dsn1; (Welburn et al., 2010)) or GFP (to detect Mis12-GFP-FKBP). Representative images (main panels) and magnified views of kinetochores (insets) are shown. Dsn1 phosphorylation was quantified from ≥20 kinetochores of 10 cells per condition and compared using one-way ANOVA and Kruskal-Wallis *post hoc* tests. Error bars indicate SEM. See also Figure S1.

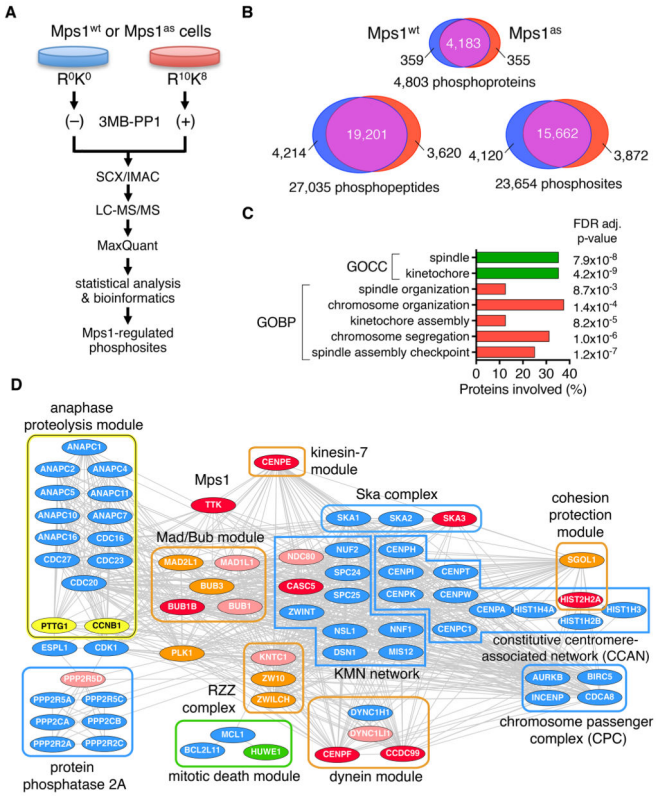

Figure 2. Global phosphoproteomics reveals sites of Mps1-regulated phosphorylation at the outer kinetochore

(A) SILAC-based strategy for systematic discovery of Mps1 substrates and effectors. Mps1^{wt} and Mps1^{as} human retinal pigment epithelial cells (Maciejowski et al., 2010) were grown in medium containing light (Arg^{0} and Lys^{0}) or heavy (Arg^{10}Lys^{8}) amino acids, synchronized in mitosis with nocodazole, then treated with or without 3MB-PP1 (plus nocodazole and MG132) for 2 hours. Tryptic phosphopeptide samples were prepared by strong cation exchange (SCX) fractionation and enrichment by immobilized metal affinity chromatography (IMAC), followed by LC-MS analysis and MaxQuant data processing (Oppermann et al., 2012). (B) Summary of large-scale phosphoproteomics data collected for Mps1^{wt} and Mps1^{as} cells. Four biological replicates were analyzed for each cell line. Only phosphosites that could be quantified and assigned to specific serine, threonine or tyrosine residues with a localization probability of at least 0.75 (class I sites) were counted (Olsen et al., 2006). (C) Gene ontology (GO) term enrichment analysis on Mps1-regulated phosphoproteins. P-values were computed by Fisher's exact test and corrected using the Benjamini-Hochberg FDR. (D) Functional association networks were retrieved from the STRING database and visualized in Cytoscape (Shannon et al., 2003). Mps1-regulated phosphoproteins quantified in at least two experimental runs per cell line are highlighted in red (decreased phosphorylation) and green (increased phosphorylation), while those quantified in fewer runs are in pink (decreased phosphorylation). Proteins and complexes with Mps1-dependent kinetochore localization (Hewitt et al., 2010; Kwiatkowski et al., 2010; Maciejowski et al., 2010; Santaguida et al., 2010) are marked in orange. APC/C^{Cdc20}

substrates securin (PTTG1) and cyclin B1 (CCNB1) are in yellow. All other proteins in the network are in blue. See also Figure S2 and Tables S1–S3.

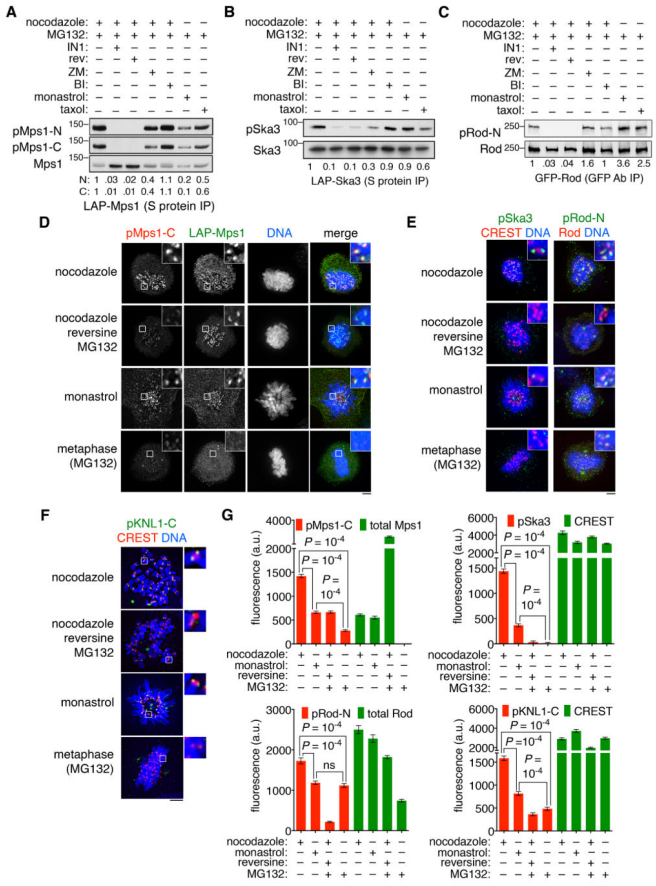

Figure 3. Mps1 substrate phosphorylation is sensitive to microtubule attachment and tension

HeLa cells expressing LAP-tagged Mps1 or Ska3 (A and B) or GFP-tagged Rod (C) were synchronized in mitosis with nocodazole, shaken off, and transferred into medium containing the indicated compounds for two hours. Inhibitors selective for Mps1 (reversine and IN-1) (Kwiatkowski et al., 2010; Santaguida et al., 2010), Aurora B (ZM447439) (Ditchfield et al., 2003), and Plk1 (BI-2536) (Lenart et al., 2007) have been described. Tagged proteins were purified from mitotic lysates using S-protein-agarose (A–B) or GFP antibody-coupled magnetic beads (C) and analyzed by Western blotting. Phosphospecific and total protein band intensities were quantified and used to compute relative phosphorylation ratios, expressed as a fraction of the no-kinase-inhibitor control (lane 1). Consistent results were obtained in at least two separate experiments. (D–F) RPE cells were treated with the indicated compounds for two hours, then fixed and permeabilized concurrently (D–E) or pre-extracted before fixation and immunostaining (F). Maximum-intensity projections of deconvolved z-stacks and magnified views of individual kinetochores are shown. Images are representative of three experiments. (G) Fluorescence intensities were measured from 200 to 250 kinetochores per condition and compared using two-way ANOVA and Sidak *post hoc* tests. Consistent results were obtained in three experiments. Error bars indicate SEM. See also Figure S3.

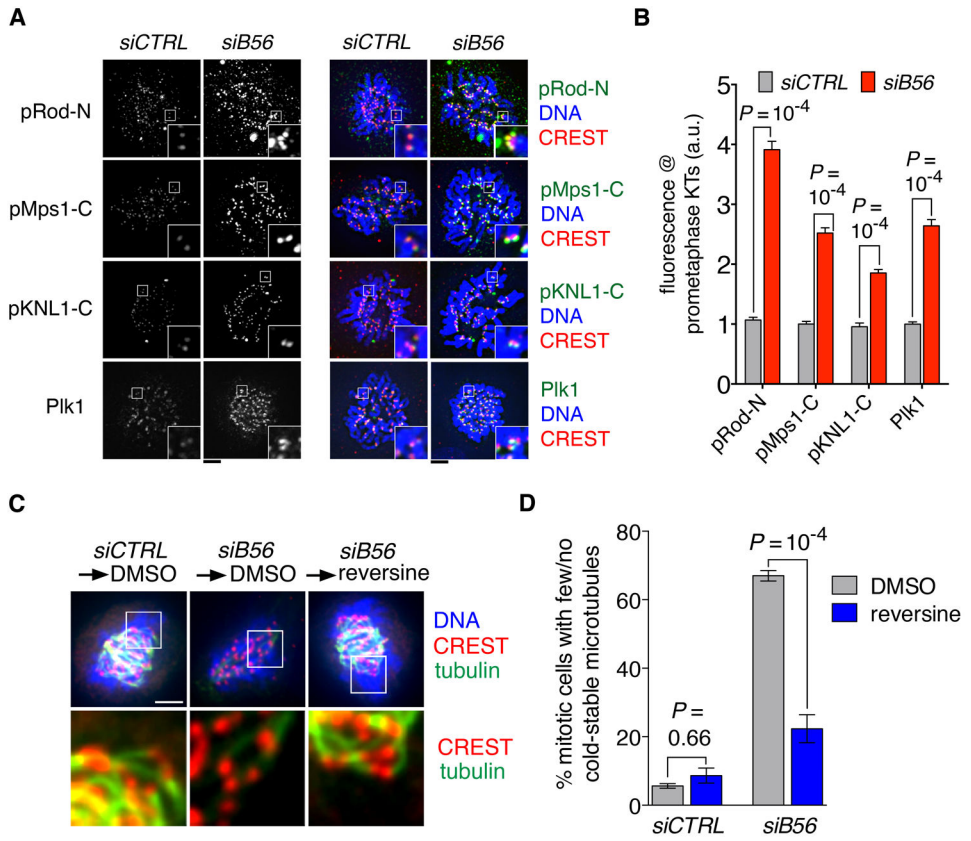

Figure 4. B56-PP2A phosphatases counteract the attachment-destabilizing activity of Mps1

(A and B) PP2A-B56 reduces Mps1-dependent phosphorylation at prometaphase kinetochores. RPE cells were transfected with a nontargeting control siRNA (*siCTRL*) or an siRNA pool targeting all B56 subunits (*siB56*). Maximum-intensity projections of deconvolved z-stacks (main panels) and magnified views of individual kinetochores (insets) are representative of two experiments. Plk1 enrichment at kinetochores was used as a positive control for PP2A-B56 depletion (Foley et al., 2011). Fluorescence intensities were measured from 59 to 113 kinetochores per condition and compared using two-way ANOVA and Sidak *post hoc* tests. Error bars indicate SEM. (C and D) Mps1 inhibition stabilizes kinetochore-microtubule attachments in PP2A-B56-deficient cells. Control and B56-depleted cells were treated with MG132 for 20 minutes, followed by addition of 200 nM reversine (rev) or solvent (DMSO) for 50 minutes. Specimens were incubated on ice for 10 minutes before fixation, processed for IFM, and scored visually. Maximum-intensity projections and magnified views of individual kinetochores (insets) are representative of three experiments. The fraction of cells with few/no cold-stable microtubules was determined in three experiments ($n \geq 40$ cells per condition per experiment) and compared using one-way ANOVA and Sidak *post hoc* tests. Error bars indicate SEM from three experiments.

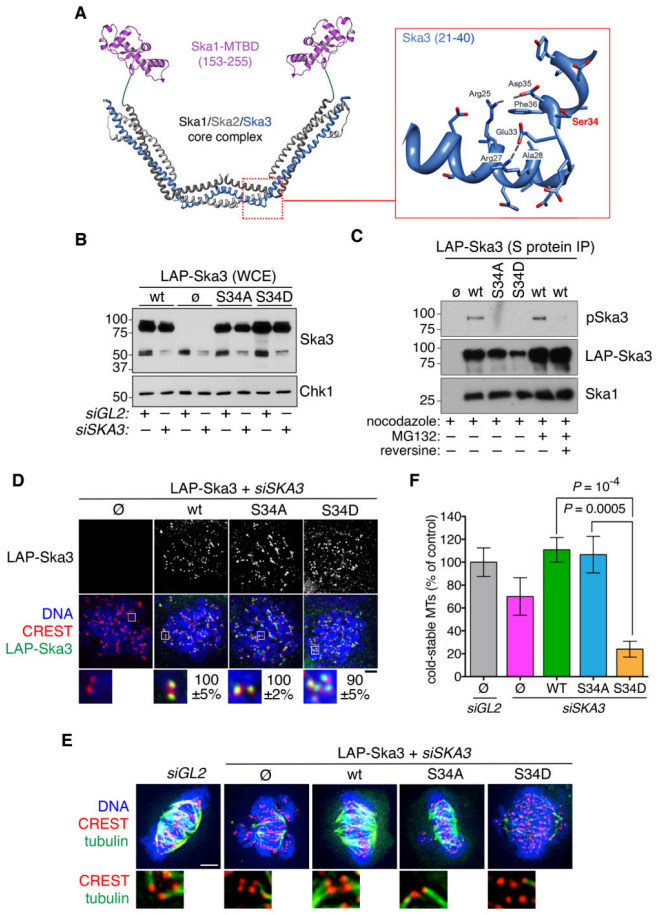

Figure 5. Mps1 destabilizes kinetochore-microtubule attachments by phosphorylating the hinge region of the Ska complex

(A) Structures of the Ska1 microtubule binding domain (MTBD) (Abad et al., 2014) and the Ska1/2/3 core complex (Jeyaprakash et al., 2012). Inset displays a magnified view of the hinge region, with serine 34 on Ska3 labeled in red. (B) HeLa cells bearing the indicated LAP-Ska3 transgenes were transfected with a 3′ UTR-specific siRNA (*siSKA3*) or luciferase-specific siRNA (*siGL2*) as a negative control, then harvested 72 hr later and analyzed by Western blotting. Chk1 was used a loading control. Results are representative of two experiments. (C) HeLa cells transgenic for LAP-Ska3 were synchronized in mitosis with nocodazole and harvested immediately (wt, S34A, and S34D; lanes 1–3), or after further treatment with MG132 (wt + MG, lane 4) or MG132 and reversine (wt + rev, lane 5) for 2 hours. LAP-Ska3 was precipitated with S-protein-agarose and analyzed by Western blotting to assess its phosphorylation state and binding to Ska1. Results are representative of three independent experiments. (D) *SKA3*-depleted HeLa cells were treated with nocodazole for 2 hr and analyzed by IFM to detect LAP-Ska3 (green) or CREST (red). Images are representative of three experiments. Kinetochore targeting of LAP-Ska3 is reported as a percentage ± SEM of the wildtype control. (E and F) Control and *SKA3*-depleted HeLa cells were treated with MG132 for 50 minutes, incubated on ice for 10 minutes, and analyzed by IFM as shown. Images shown are representative of three experiments. Cold-stable microtubules were quantified from 8 to 12 cells per condition and compared using one-way

ANOVA and Kruskal-Wallis *post hoc* test. No cold-stability defect was observed in the absence of Ska3 depletion, indicating that the S34D allele acts recessively.

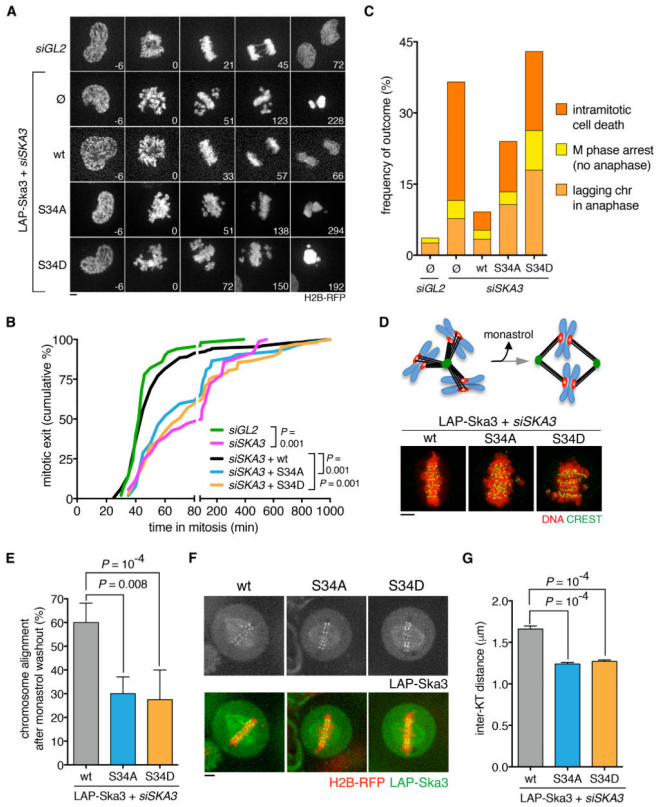

Figure 6. Regulated phosphorylation and dephosphorylation of the Ska complex hinge are required for accurate chromosome segregation

(A) HeLa cells transgenic for LAP-Ska3 and H2B-RFP were transfected with siRNAs and followed by spinning disk microscopy. Time relative to nuclear envelope breakdown (NEBD) is indicated on each image and representative of at least three experiments per condition. (B) The length of M phase (from NEBD to mitotic exit or cell death) was quantified from 104 to 208 cells in three experiments and compared using one-way ANOVA and Kruskal-Wallis *post hoc* test. (C) Cells analyzed in (B) were also scored for their eventual fates (persistent mitotic arrest, cell death, or anaphase with or without lagging chromosomes). (D and E) HeLa cells reconstituted with wildtype or mutant LAP-Ska3 were treated with monastrol for 2 hours. Following washout, cells were incubated in MG132 for 60 minutes, then fixed and analyzed by IFM. Images are representative of two experiments (n = 40 to 100 cells analyzed per condition; *P*-values computed using Fisher's exact test). (F and G) Live imaging of LAP-Ska3 and H2B-RFP in cells reaching metaphase after endogenous *SKA3* depletion. Inter-kinetochore distances were measured from 105 to 130 sister kinetochore pairs (6 to 10 cells per condition) and compared using one-way ANOVA and Kruskal-Wallis *post hoc* test.

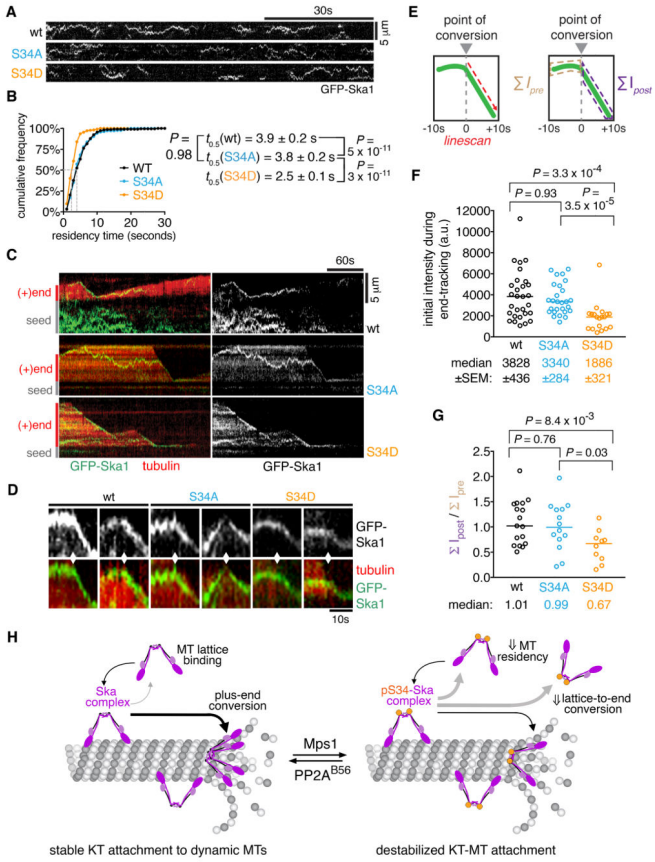

Figure 7. Phosphomimetic hinge mutation decreases the Ska complex's microtubule residency time and impedes its lattice-to-end conversion on disassembling microtubules

(A) Kymographs of GFP-labeled wildtype and hinge-mutant Ska complexes on GMP-CPP stabilized microtubules, demonstrating 1-D diffusion on the lattice. (B) Cumulative plot of microtubule residency times for SKA^{wt} (n=223), SKA^{S34A} (n=208), and SKA^{S34D} complexes (n=207). Half-lives ($t_{0.5}$) of each complex were compared using a Mann-Whitney U test. (C) Kymographs of GFP-labeled Ska complexes on dynamic X-rhodamine labeled microtubules, demonstrating end-tracking behavior. Note that microtubule seeds were labeled in the far-red channel and hence not visible. (D) Magnified views of lattice-to-end conversion events (arrowheads), at which Ska complexes switched from 1-D diffusion to processive tracking of the depolymerizing plus end. (E) Scheme for quantitative analysis of lattice-to-end conversion events. The initial intensity of end-tracking Ska complexes during the first 10 seconds of end-tracking (left panel) and their change in intensity relative to pre-conversion Ska complexes (right panel) were determined as shown. (F) Median intensities of SKA^{wt} (n=29), SKA^{S34A} (n=27), and SKA^{S34D} particles (n=19) that initiate end tracking. Statistical comparisons were made using a Mann Whitney U test. (G) Integrated post-conversion (ΣI_{post}) and pre-conversion (ΣI_{pre}) intensities were determined for SKA^{wt} (n=18), SKA^{S34A} (n=14), and SKA^{S34D} particles (n=13). Ratios below 1 indicate loss of Ska complexes during lattice-to-end conversion. Statistical comparisons were made using a Mann Whitney U test. (H) Hinge phosphorylation promotes the Ska complex's dissociation

from microtubules and impedes its conversion from lattice diffusion to processive end-tracking during microtubule depolymerization. See also Figure S4.